Homozygous ALS-linked mutations in TARDBP/TDP-43 lead to progressive synaptic dysfunction in human iPSC-derived motor neurons

Sarah Lépine[1,2], Angela Nauleau-Javaudin[1,3], Eric Deneault[4], Carol X.-Q. Chen[1], Narges Abdian[1], Anna Krystina Franco-Flores[1], Ghazal Haghi[1], María José Castellanos-Montiel[1], Gilles Maussion[1], Mathilde Chaineau[1,*], and Thomas M. Durcan[1,*]

[1]Early Drug Discovery Unit (EDDU), The Neuro-Montreal Neurological Institute and Hospital, Department of Neurology and Neurosurgery, McGill University, Montreal, QC, H3A 1A1, Canada
[2]Faculty of Medicine and Health Sciences, McGill University Montreal, QC, H3G 2M1, Canada
[3]Faculty of Medicine, Université de Montréal, Montreal, QC, H3C 3J7, Canada
[4]Centre for Oncology, Radiopharmaceuticals and Research; Biologic and Radiopharmaceutical Drugs Directorate, Health Products and Food Branch, Health Canada, Ottawa, ON, K1A 0K9, Canada

*Correspondence: thomas.durcan@mcgill.ca; mathilde.chaineau@mcgill.ca

Summary

Cytoplasmic mislocalization and aggregation of the RNA-binding protein TDP-43 is a pathological hallmark of the motor neuron (MN) disease amyotrophic lateral sclerosis (ALS). Furthermore, while mutations in the *TARDBP* gene (encoding TDP-43) have been associated with ALS, the pathogenic consequences of these mutations remain poorly understood. Using CRISPR/Cas9, we engineered two homozygous knock-in iPSC lines carrying mutations in *TARDBP* encoding TDP-43^{A382T} and TDP-43^{G348C}, two common yet understudied ALS TDP-43 variants. MNs differentiated from knock-in iPSCs had normal viability and displayed no significant changes in TDP-43 subcellular localization, phosphorylation, solubility, or aggregation compared with isogenic control MNs. However, our results highlight synaptic impairments in both TDP-43^{A382T} and TDP-43^{G348C} MN cultures, as reflected in synapse abnormalities and alterations in spontaneous neuronal activity. Collectively, our findings argue that MN dysfunction precedes the occurrence of TDP-43 pathology and neurodegeneration in ALS, and further implicates synaptic and excitability defects in the pathobiology of this disease.

Highlights

- MNs differentiated from knock-in iPSCs do not display a neurodegenerative phenotype.
- Mutant MNs do not show TDP-43 pathology.
- TDP-43 variants lead to a progressive decline in spontaneous neuronal activity.
- Functional impairments are accompanied by abnormal synaptic marker expression.

eTOC blurb

Using CRISPR/Cas9-edited iPSCs, Lépine et al. demonstrate that ALS TDP-43 variants (TDP-43^{A382T} and TDP43^{G348C}) lead to alterations in spontaneous neuronal activity and synaptic

abnormalities in the absence of TDP-43 mislocalization, aggregation, or neurodegeneration. These findings imply that TDP-43 pathology is not required to induce MN dysfunction and support the presence of early synaptic impairments prior to MN loss in ALS.

Keywords: TDP-43; TARDBP; amyotrophic lateral sclerosis; CRISPR/Cas9; gene editing; induced pluripotent stem cells; disease modeling; motor neuron; synapse; multielectrode array

Introduction

Amyotrophic lateral sclerosis (ALS) is a neurodegenerative disorder characterized by the progressive loss of motor neurons (MNs) in the brain and the spinal cord, resulting in weakness and paralysis that is usually fatal within two to four years after onset (Moura et al., 2015). While about 10% of ALS cases follow a pattern of inheritance (termed familial ALS (fALS)), the majority of cases occur in the absence of a clear family history (sporadic ALS (sALS)). Overall, it is estimated that 15-20% of cases have a known genetic cause (Kenna et al., 2013). The *TARDBP* gene (encoding TDP-43) is among the most commonly mutated ALS-associated genes after *C9ORF72*, *SOD1* and *FUS*, with nearly 40 missense mutations identified in patients to date (ALSoD database; https://alsod.ac.uk/). At the neuropathological level, the cytoplasmic mislocalization and aggregation of TDP-43 is a signature feature of ALS. These pathological changes, known as TDP-43 pathology, are observed in post-mortem tissues of >95% of patients (Arai et al., 2006; Mackenzie et al., 2007; Neumann et al., 2006), suggesting that convergent mechanisms of TDP-43 dysfunction are involved in both familial and sporadic disease. Thus, identifying the mechanisms through which TDP-43 dysregulation contributes to disease pathogenesis is of foremost importance in developing new therapeutics for ALS.

TDP-43 is a DNA/RNA binding protein involved in several steps of RNA processing including transcription, splicing, RNA transport, and translation (Alami et al., 2014; Buratti and Baralle, 2001; Coyne et al., 2014; Ou et al., 1995). Early efforts to decipher the pathological roles of TDP-43 in ALS have primarily focused on overexpression and loss-of-function models and demonstrated that TDP-43 levels must be tightly regulated for it to exert its normal cellular functions. Indeed, genetic ablation of *TARDBP* is lethal during embryogenesis (Kraemer et al., 2010; Sephton et al., 2010), and acute TDP-43 depletion (i.e., via conditional knockout or RNA interference) leads to neurodegeneration and ALS-like manifestations in mice (Iguchi et al., 2013; Wu et al., 2012; Yang et al., 2014). Similarly, overexpression of ALS-associated TDP-43

variants, or even the wild-type protein, exerts deleterious effects across species, including motor deficits, shortened lifespan, and MN loss (Armstrong and Drapeau, 2013; Estes et al., 2011; Kabashi et al., 2010; Mitchell et al., 2015; Shan et al., 2010). Given the potential confounding effects of overexpression strategies, discerning the pathological contributions of *TARDBP* mutations has been challenging.

Progress in induced pluripotent stem cell (iPSC) and gene editing technologies now offer an unprecedented opportunity to model ALS with human disease-relevant cells. Our group and others have established robust workflows for quality control, gene editing, and differentiation of iPSCs into several cell types, including MNs (Chen et al., 2021; Deneault et al., 2022; Du et al., 2015). In recent years, a number of iPSC-derived models have been generated to assess the effects of *TARDBP* mutations expressed at endogenous levels *in vitro* (reviewed in (Hawrot et al., 2020)). Although both gain- and loss-of-function mechanisms have been proposed, the pathogenic properties of ALS TDP-43 variants remain poorly understood. In particular, the pathologic manifestations of the TDP-43^{A382T} and TDP-43^{G348C} variants - the first and third most frequent ALS variants of TDP-43, respectively (ALSoD database; https://alsod.ac.uk/) - have not yet been fully characterized in a human model system.

To address this gap, we utilized CRISPR/Cas9 to generate two homozygous knock-in iPSC lines carrying point mutations in *TARDBP* coding for TDP-43^{A382T} or TDP-43^{G348C}. We found that these mutations did not cause overt neurodegeneration nor TDP-43 aggregation or cytoplasmic mislocalization. Furthermore, mutant MNs did not recapitulate other biochemical hallmarks of pathologically altered TDP-43, including phosphorylation, C-terminal cleavage, and accumulation of detergent-insoluble species. Despite the apparent absence of TDP-43 pathology, our results highlight synaptic abnormalities and decreased neuronal activity in mutant MNs, pointing to synaptic dysfunction as an early event in ALS pathogenesis.

Results

Generation of *TARDBP* knock-in iPSCs lines using CRIPSR/Cas9

The vast majority of *TARDBP* mutations cluster in exon 6 of the gene, which encodes the protein's C-terminal domain. Using CRISPR/Cas9 technology, we edited a well characterized healthy control iPSC line (i.e., AIW002-02) (Chen et al., 2021) to generate two homozygous knock-in *TARDBP* iPSC lines expressing TDP-43^{A382T} or TDP-43^{G348C} (**Table S1**). Gene editing was performed by nucleofection of (i) the Cas9 nuclease, (ii) the single guide RNA (sgRNA) targeting the edit site of *TARDBP* (exon 6), and (iii) the single-stranded donor oligonucleotide (ssODN) carrying the mutation and the homology arms to enable integration into the genome via homology-directed repair (**Figure 1A; Table S2**). Successful introduction of the mutations and homozygosity of the iPSC lines were confirmed by digital droplet PCR (ddPCR) and Sanger sequencing (**Figures 1B, S1A and S1B; Table S3**). The pluripotency of gene-edited iPSCs was verified by performing immunocytochemistry for pluripotency-associated markers Nanog, TRA-1-60, SSEA-4, and Oct-3/4 (**Figure S2B**). Genome stability testing confirmed that *TARDBP* knock-in iPSC lines maintained normal karyotypes and chromosome copy numbers (**Figures S2C and S2D**). Isogeneity with the parental control iPSC line was verified using short-tandem repeat (STR) profiling (**Figure S2E**).

TARDBP mutations do not impair normal differentiation of iPSCs into MNs

The two knock-in iPSC lines (TDP-43^{A382T} and TDP-43^{G348C}) and the AIW002-02 parental isogenic control line were differentiated into MNs using a previously published protocol that mimics MN differentiation during development (Deneault et al., 2022) (**Figure 1C**). Cells were harvested at multiple timepoints to characterize the differentiation process and validate their identity. iPSCs were initially induced into neuroepithelial progenitors (NEPs) via dual-SMAD

signaling inhibition, followed by specification into MN progenitor cells (MNPCs). MNPCs showed immunoreactivity for progenitor markers OLIG2, PAX6, and Nestin without significant differences between mutant and isogenic control cultures (**Figure S3A-S3D**). MNPCs were then cryopreserved or plated for final differentiation into MNs (**Video 1**). After two- and four-weeks post-plating of MNPCs, immunocytochemical analyses revealed a similar proportion of $HB9^{+}$ and $ISL1/2^{+}$ MNs as well as comparable expression of cholinergic markers ChAT and VAChT among mutant and isogenic control cultures (**Figure 1E-1I**). Quantitative PCR (qPCR) analysis examining longitudinal transcript levels of developmental markers confirmed that mutant and isogenic control cultures downregulated MNPC markers and upregulated MN markers as they differentiated into MNs (**Figure 1D**). Additionally, differentiating MNs upregulated *FOXP1* and downregulated *LHX3* (**Figure 1D**), consistent with limb-innervating lateral motor column (LMC) MN identity (Amoroso et al., 2013). LMC MNs ($FOXP1^{+}$/$LHX3^{-}$) are most susceptible to neurodegeneration in the majority of ALS patients, where disease typically first manifests by focal weakness in distal limb muscles (Masrori and Van Damme, 2020). Lastly, immunostaining with two neuronal markers (NF-H and βIII-tubulin) revealed that TDP-43 MN cultures formed a dense axonal network with similar morphological features relative to control conditions, including comparable total axonal area and branching (**Figure 2A-2F**). Overall, these results indicate that $TDP\text{-}43^{A382T}$ and $TDP\text{-}43^{G348C}$ do not impair the normal differentiation of iPSCs into MNs.

TDP-43 MN cultures maintain viability

Neurodegeneration is a core feature of ALS. For this reason, we examined whether MNs derived from *TARDBP* knock-in iPSCs were more vulnerable to cell death. We analyzed the viability of MNs differentiated for 2, 4 and 6 weeks using an ATP-based luminescent viability assay (**Figure 2G**). TDP-43 MN cultures survived at comparable levels to the isogenic control under basal conditions. Given that neurotrophic factors (NFs) are known to promote cell survival, we

hypothesized that withdrawal of NF supplementation from the differentiation medium might reveal a specific vulnerability of ALS MNs, as reported by another group with *C9ORF72* iPSC-derived MNs (Shi et al., 2019). The overall survival of MN cultures decreased by approximately 40% at 6-weeks post-plating when cells were differentiated in medium without NFs compared with complete medium, highlighting the importance of NF supplementation for long-term culture of iPSC-derived MNs. However, viability remained comparable between the mutant and control cell lines.

Next, we tested the hypothesis that TDP-43 MNs might be more vulnerable when challenged with a cellular stressor, such as glutamate. Glutamate excitotoxicity has been proposed to play a role in the pathogenesis of ALS (Blasco et al., 2014; Rothstein et al., 1992, 1995). Thus, we analyzed the viability of MN cultures treated with glutamate for 24 hours (**Figure 2H**). As expected, glutamate treatment induced MN death, as shown by a significant decrease in viability compared with vehicle-treated cultures. When comparing the survival of glutamate-treated TDP-43 MNs and isogenic control, we observed a trend towards reduced viability in both TDP-43^{A382T} and TDP-43^{G348C} MNs indicative of a potentially enhanced susceptibility to glutamate, although this effect did not reach statistical significance. Taken together, these results indicate that TDP-43 MNs did not display a neurodegenerative phenotype up to the latest timepoint investigated.

Mutant MNs do not accumulate insoluble or phosphorylated TDP-43

TDP-43 aggregates constitute the pathological hallmark of ALS, with a biochemical signature that consists of detergent-insoluble phosphorylated TDP-43 as well as C-terminal fragments of the protein (Arai et al., 2006; Mackenzie et al., 2007; Neumann et al., 2006). To assess TDP-43 levels and solubility, we performed protein fractionation of mutant and control MN cultures into total, soluble, and insoluble fractions (**Figure 3A**). Western blot analysis of total lysates showed similar TDP-43 levels between mutant and isogenic control MNs (**Figures 3G and 3H**).

Accordingly, *TARDBP* transcripts levels were also unchanged between mutant and control samples at all tested timepoints (**Figure S4A**), indicating that the mutations do not cause impairments in the autoregulatory function of TDP-43, where TDP-43 regulate levels of its own *TARDBP* transcript via a negative feedback loop (Ayala et al., 2011). When analyzing the soluble (RIPA) and insoluble (urea) protein fractions, mutant and control lysates showed comparable levels of soluble and insoluble TDP-43 (**Figures 3B-3D**), indicating a similar solubility of TDP-43^{A382T} and TDP-43^{G348C} to the wild-type protein. The C-terminal fragment of 35 kDa (CTF-35) was markedly enriched in insoluble fractions, although no differences in insoluble CTF-35 levels were observed mutant and control MNs (**Figure 3E**). Additionally, the CTF-35/TDP-43 ratio did not significantly differ (**Figure 3F**), indicating that the TDP-43 variants do not display enhanced C-terminal cleavage compared with control.

Next, we analyzed the phosphorylation state of TDP-43 using an antibody targeting phosphorylated TDP-43 (pTDP-43) (Ser409/410). Using western blotting, we found similar levels of total pTDP-43 in unfractionated lysates of mutant and control MNs (**Figures 3I and 3J**). Immunostaining showed abundant punctate pTDP-43 in the cytoplasm, with no notable differences in the abundance of pTDP-43^{+} puncta between mutant and control MNs (**Figure S4B**).

TDP-43^{A382T} and TDP-43^{G348C} do not exhibit changes in nucleocytoplasmic localization

Another prominent feature of TDP-43 pathology is mislocalization of TDP-43 in the cytoplasm. Thus, we performed nuclear/cytosolic protein fractionation experiments to quantify the distribution of TDP-43 (**Figures 4A and 4B**). Western blot analysis indicated no significant differences in TDP-43 levels in nuclear and cytosolic fractions of TDP-43 MNs compared with control (**Figures 4C and 4D**). CTF-35 was mainly recovered in cytosolic fractions, at similar

levels between samples (**Figure 4E**). The CTF-35/TDP-43 ratio was also comparable, confirming the absence of increased C-terminal cleavage in TDP-43 MNs compared with control (**Figure 4F**).

To further assess TDP-43 subcellular localization, we performed immunocytochemistry (**Figures 4G**). TDP-43 was predominantly nuclear with some signal detected in the cytoplasm. Immunocytochemical analyses revealed comparable nuclear-to-cytosolic ratios and TDP-43/Hoechst correlation coefficients between TDP-43 MNs and control, indicating similar nucleocytoplasmic localization (**Figures 4H and 4I**). These observations were recapitulated with a second TDP-43 antibody targeting the protein's N-terminus (rather than its C-terminus) (**Figures S5A-S5C**). Compared with C-terminal immunostaining, N-terminal immunostaining showed a more prominent cytosolic signal and TDP-43^{+} puncta could be observed, as previously described (Weskamp et al., 2020). However, it is worthy noting that TDP-43^{+} puncta were not detected more frequently in mutant MNs compared with control and did not co-localize with pTDP-43^{+} puncta, in line with recent findings (Ratti et al., 2020). As such, we hypothesize that TDP-43^{+} puncta may represent RNA granules rather than proper aggregates. Taken together, these results indicate that mutant MNs do not exhibit TDP-43 pathology as observed in post-mortem tissues.

Progressive decline in spontaneous neuronal activity in TDP-43 MNs

To assess the activity and functionality of MNs, we performed electrophysiological profiling of MN cultures using multielectrode array (MEA) over a span of 8 weeks post-plating. We observed progressive alteration of spontaneous neuronal activity in TDP-43^{A382T} and TDP-43^{G348C} MNs with prolonged time in culture, as shown by a significant decline in mean firing rate compared with isogenic control MNs 5 weeks post-plating (**Figure 5B**). Additionally, we noted fewer active

electrodes in TDP-43 MN cultures compared with control cultures despite a similar distribution of cells over the electrodes (**Figure 5A and 5C; Video 2**), indicating that they are more electrophysiologically silent. Among active electrodes, however, the burst frequency, number of spikes per burst, and burst duration remained unchanged between TDP-43 and control MN cultures (**Figure S5A, S5B and S5C**). Treatment with the sodium-channel blocker tetrodotoxin (TTX) abolished neuronal activity, thereby confirming that the recorded signals are due to action potentials and not artifacts (**Figure 5D**).

TDP-43 MNs exhibit abnormal pre- and postsynaptic puncta

To further study the mechanisms underlying altered neuronal activity, we examined whether TDP-43 MNs would display changes in synapse number and morphology. We performed co-immunostaining for presynaptic (synapsin I) and postsynaptic (PSD95) compartments in MN cultures differentiated for 6 weeks (**Figure 6A**) and analyzed mean puncta count, size, and signal intensity. We found no significant change in the number of synapsin I^+ puncta between TDP-43 MNs and control (**Figure 6B**). However, the average size of synapsin I^+ puncta was increased in TDP-43^{A382T} MNs, but not TDP-43^{G348C} MNs, compared with control (**Figure 6C**). We also observed a significant decrease in synapsin I^+ puncta mean intensity in TDP-43^{G348C} MNs compared with TDP-43^{A382T} and control MNs (**Figure 6D**). When analyzing PSD95 immunostaining, the number of $PSD95^+$ puncta was significantly decreased in TDP-43^{A382T} MNs and we observed a trend towards fewer $PSD95^+$ puncta in TDP-43^{G348C} compared with control (**Figure 6E**). Both TDP-43^{A382T} MNs and TDP-43^{G348C} MNs displayed significantly larger $PSD95^+$ puncta sizes than control MNs (**Figure 6F**). The mean intensity of $PSD95^+$ puncta was not significantly different between TDP-43 MNs and control, although a trend towards decreased $PSD95^+$ puncta intensity was observed in TDP-43^{G348C} MNs (**Figure 6G**). We also analyzed the colocalization of both synapsin I and PSD95 markers. We found no significant change in the

number of synapsin I^+/$PSD95^+$ puncta between TDP-43 MNs and control (**Figure 6H**). However, the size of synapsin I^+/$PSD95^+$ puncta was significantly larger in TDP-43^{A382T} MNs, but not TDP-43^{G348C} MNs, compared with control (**Figure 6I**). Based on these observations, we conclude that TDP-43 MNs exhibit synaptic defects.

TDP-43 variants perturb the expression of synaptic proteins post-transcriptionally

Earlier MEA experiments implied that alterations in activity manifest after prolonged time in culture, leading us to analyze protein levels of presynaptic (synapsin I, synaptophysin) and postsynaptic (PSD95) markers at several timepoints (**Figure 7A**). Western blot analysis indicated increased levels of PSD95 at 2 weeks post-plating in both TDP-43 MN cultures compared with control, but those levels were not significantly different at other timepoints (**Figure 7B**). We observed comparable levels of synaptophysin between samples at all timepoints (**Figure 7D**). Levels of synapsin I, however, were significantly depleted at 6-weeks post-plating, coinciding with the observed decline in mean firing rate (**Figure 7C**). We next sought to determine whether dysregulation of synaptic marker expression occurs at the transcriptional level (**Figure 7E-7G**). Despite the prominent decrease in synapsin I protein at 6-weeks post-plating, *SYN1* transcript levels, however, remained unchanged between TDP-43 and control MNs at this timepoint (**Figure 7F**). These results imply that TDP-43 variants perturb the expression of synapsin I post-transcriptionally. In summary, we find that impairments in spontaneous neuronal activity are reflected by abnormal synaptic marker expression.

Discussion

The detection of TDP-43 pathology in almost all ALS cases, along with the identification of disease-causing mutations in the *TARDBP* gene, underscores a central role of TDP-43 dysregulation in ALS pathobiology. Yet, the mechanisms by which *TARDBP* mutations

contribute to MN dysfunction and neurodegeneration remains poorly understood. In this study, we harnessed iPSC and CRIPSR/Cas9 gene editing technologies to study the impact of *TARDBP* mutations in a more physiological context. Due to our lack of TDP-43 patient samples, we edited a healthy control iPSC line to generate two homozygous knock-in iPSC lines with *TARDBP* mutations encoding the TDP-43^{A382T} and TDP-43^{G348C} variants, respectively, thereby allowing the comparison of cellular phenotypes between gene-edited cells and their parental cell line. This isogenic experimental design (where cell lines share the same genetic information except for the mutation of interest) is critical to eliminate variability due to genetic background, reprogramming, and differentiation efficiencies, which can affect the reproducibility of experiments in iPSC studies (Kilpinen et al., 2017; Rouhani et al., 2014). One limitation of this study, however, is that since the mutant iPSC lines were not derived from patient cells, they may lack ALS genetic modifiers naturally present in patients' genotypes, which could be important contributors to the disease phenotypes.

With these edited lines, we tested the hypothesis that MNs differentiated from the *TARDBP* knock-in iPSCs would manifest features of ALS *in vitro* when cultured for a prolonged period. We found that TDP-43 MNs did not exhibit a cell death phenotype up to 6 weeks of maturation, the latest timepoint investigated. These observations are consistent with earlier reports in which differences in viability between MN cultures derived from *TARDBP* mutant and control iPSC lines were not detected under basal culture conditions (Devlin et al., 2015; Egawa et al., 2012; Krach et al., 2022; Seminary et al., 2018; Zhang et al., 2013). Some noted enhanced stress-induced neuronal death following treatment with compounds such as sodium arsenite, staurosporine, MG-132 or LY294002 (a selective PI3K inhibitor) (Bilican et al., 2012; Egawa et al., 2012; Sun et al., 2018; Zhang et al., 2013), suggesting some inherent vulnerability conferred by the mutations. Our work showed only trends towards increased susceptibility of mutant MNs to glutamate toxicity. The absence of overt MN loss may reflect the immaturity of MNs at the

timepoints examined. In future studies, overcoming the challenges associated with long-term culture of MNs in monolayers (i.e., cell clumping and detachment) or use of three-dimensional culture models (i.e., spheroids, organoids) (Castellanos-Montiel et al., 2023; de Majo et al., 2023; Pereira et al., 2021) may enable neurodegeneration to be observed after several months of culture, without the need for exogenous treatments with stressors to elicit a phenotype. Alternatively, transcription factor-mediated transdifferentiation towards specific neurons, avoiding intermediate proliferative pluripotent stem cell stage, may help retaining specific age-related and epigenetic features involved in neurodegenerative disorders (Mollinari et al., 2018).

As aging is a strong risk factor for ALS, enhancing the maturation of MN cultures may also accelerate the manifestation of end-stage disease features, such as TDP-43 pathology. Here, we show that mutant MNs did not robustly display cytoplasmic mislocalization, aggregation, or accumulation of insoluble TDP-43 under basal conditions, in line with most recent reports of iPSC-derived MNs carrying *TARBDP* mutations (Bossolasco et al., 2018; Dafinca et al., 2020; Imaizumi et al., 2022; Klim et al., 2019; Krach et al., 2022; Kreiter et al., 2018; Ratti et al., 2020; Wang et al., 2013). Some studies, in contrast, found that mutant MNs recapitulate partial aspects of TDP-43 pathology *in vitro* (Bilican et al., 2012; Egawa et al., 2012; Fazal et al., 2021; Fujimori et al., 2018; Smith et al., 2021; Sun et al., 2018), sometimes reporting enhanced cytoplasmic distribution of TDP-43 (albeit without nuclear depletion), increased levels of insoluble TDP-43 and lower molecular weight species and/or, in few instances, detection of “preinclusion-like aggregates” by immunocytochemistry or electron microscopy. These discrepancies, together with the absence of overt neurodegeneration, suggest that iPSC-derived MNs may model early stages of ALS.

One prominent finding of the present study is the progressive decline in spontaneous neuronal activity in TDP-43^{A382T} and TDP-43^{G348C} MNs after several weeks in culture. Although we noted abnormal pre- and postsynaptic puncta, we found no significant changes in the number of

synapsin I^+/$PSD95^+$ puncta between TDP-43 MNs and control, indicating that altered neuronal activity is not due to a failure of synaptogenesis nor synaptic loss. These results suggest that functional alterations in synaptic activity may arise before the physical disruption of synapses in ALS. Indeed, previous studies of animal models and ALS patients have implicated excitability defects in this disease (Martínez-Silva et al., 2018; Vucic et al., 2008). Additionally, neuronal hypoexcitability, sometimes preceded by transient early hyperexcitability, has been described in iPSC-derived neurons with mutations in *TARDBP* (Dafinca et al., 2020; Devlin et al., 2015; Zhang et al., 2013). A possible progression from initial hyper- to hypoexcitability is also supported by studies in ALS mouse models (Delestrée et al., 2014; Fuchs et al., 2013) and iPSC-derived models carrying mutations in *C9ORF72* (Dafinca et al., 2020; Devlin et al., 2015; Sareen et al., 2013; Zhao et al., 2020), *SOD1* (Kim et al., 2020; Naujock et al., 2016; Wainger et al., 2014) and *FUS* (Guo et al., 2017; Naujock et al., 2016), depending on the timepoint examined.

Accumulating evidence suggests that TDP-43 is involved in synaptic functions, both at central and neuromuscular synapses (reviewed in (Gulino, 2023; Lépine et al., 2022; Ling, 2018)). Pathologically altered TDP-43 has been shown to perturb the expression of synaptic genes in ALS mouse models and patients (Brown et al., 2022; Ma et al., 2022; Mishra et al., 2007; Polymenidou et al., 2011). Here, we found that synapsin I protein levels, but not *SYN1* transcript levels, were depleted in TDP-43^{A382T} and TDP-43^{G348C} MNs after 6 weeks post-plating, which was coincident with the decline in neuronal activity. These results imply that differences in synapsin I levels result from a post-transcriptional mechanism, such as impairments in mRNA transport, translation and/or mRNA sequestration by TDP-43, as described by several groups (Alami et al., 2014; Altman et al., 2021; Coyne et al., 2017; Zuo et al., 2021). Further research will be required to elucidate the molecular mechanisms by which *TARDBP* mutations lead to

decreased synapsin I expression, potentially contributing to functional defects (Baldelli et al., 2007; Rosahl et al., 1995).

Overall, our findings indicate that TDP-43 pathology is not required to induce MN dysfunction and support the presence of early synaptic impairments prior to MN loss in ALS. As the synapse emerges as a promising therapeutic target for ALS, neuronal activity and synapse integrity may serve as disease-relevant phenotypic readouts for drug discovery.

Experimental Procedures

See further details in the Supplemental Experimental Procedures.

Resource Availabilities

Corresponding author. Further information and requests should be directed to the lead contact, Thomas M. Durcan (thomas.durcan@mcgill.ca).

Materials availability. Cell lines generated in this study will be made available on request, under the open science framework of the Neuro, and through a cost recovery model.

Data and code availability. Derived data supporting the findings of this study are available from the lead contact upon request.

iPSC lines and culture

The use of human cells in this study was approved by McGill University Health Center Research Ethics Board (DURCAN_iPSC / 2019-5374). To knock-in selected mutations, we used the previously characterized control cell line AIW002-02, reprogrammed from peripheral blood mononuclear cells (PBMCs) of a 37-year-old Caucasian male, as previously described (Chen et al., 2021). A summary of the iPSC lines used can be found in **Table S1**. iPSCs were maintained on dishes coated with Matrigel (Corning Millipore) in mTeSR1 (StemCell Technologies) and passaged at 80% confluence using Gentle Cell Dissociation Reagent (StemCell Technologies). Cultures were routinely tested for mycoplasma using the MycoAlert Mycoplasma Detection kit (Lonza).

CRISPR/Cas9 genome editing and validation

To genetically edit *TARDBP*, CRISPR reagents were transfected into iPSCs using the P3 Primary Cell 4D Nucleofector™ X Kit S (Lonza), as previously described (Deneault et al., 2022). Briefly, iPSCs at 50% confluency were dissociated with Accutase (StemCell Technologies) and 500,000 cells were resuspended in 25 µL of Cas9: sgRNA ribonucleoprotein (RNP)-ssODN-buffer mix, consisting of 1 µL of Cas9 protein (stock 61 µM), 3 µL of sgRNA (stock 100 µM), and 1 µL of ssODNs (stock 100 µM) in 20 µL of nucleofection buffer P3. The reaction mixture was then electroporated using the CA137 program in a Nucleofector 4D device. The sequences of the sgRNAs and ssODNs used are provided in **Table S2**.

After limiting dilution, gene-edited clones were identified by ddPCR (QX200™ Droplet Reader, Bio-Rad). The detection of the modified nucleotide by ddPCR was based on a TaqMan® assay including two PCR primers and two DNA probes fused with different fluorophores (FAM and HEX), with one probe specific to the original allele and the other probe to the edited allele. Locked Nucleic Acid (LNA®) probes were designed following the manufacturer's criteria. Sequence integrity of successful clones was assessed using Sanger sequencing. The sequences of the primers and probes used for ddPCR, and Sanger sequencing are provided in **Table S3**.

Statistical tests

Biological replicates were defined as independent differentiations unless otherwise specified. Statistical analyses were performed with the GraphPad Prism 9.3.0 software. Data distribution was assumed to be normal although this was not formally tested. Differences between multiple groups were analyzed using one-way or two-way analysis of variance (ANOVA) tests. Means

and standard errors of the mean were used for data presentation. Significance was defined as $p<0.05$.

Acknowledgements

We acknowledge Dr. Vincent Soubannier for training and guidance on microscopy image acquisition and analysis, Ghislaine Deyab for guidance on MEA data analysis, Shuming Li for programming the macro for visualization of MEA data, and Dr. Mark R. Aurousseau for his contribution to the development of the glutamate assay. We are also grateful to Dr. Gary A.B. Armstrong for creative discussions and his advice and to Dr. Lenore K. Beitel for proofreading the manuscript. SL was supported by the Faculty of Medicine and Health Sciences of McGill University. TMD acknowledges support from the Canada First Research Excellence Fund, awarded through the Healthy Brains, Healthy Lives initiative at McGill University, the CQDM FACs program, and the US Department of Defense ALS Research Program support. All figures and schematics were created with BioRender.com.

Author contributions

SL, MC, and TMD conceived the project. SL, MC, GM, and TMD designed experiments. ED designed and performed editing of the *TARDBP* knock-in iPSC lines. CXQC and NA performed iPSC characterization and quality control. SL, AKFF, GH, and MJCM performed inductions of iPSCs to MNPCs. MC and GH developed the glutamate viability assay. SL performed experiments, with support from ANJ and AKFF. SL performed data analysis. SL prepared the original draft of the manuscript. SL, MC, and TMD reviewed and edited the manuscript. TMD supervised all aspects of the study. All authors reviewed and commented on the manuscript.

Declaration of interests

The authors declare no competing interests.

References

Alami, N.H., Smith, R.B., Carrasco, M.A., Williams, L.A., Winborn, C.S., Han, S.S.W., Kiskinis, E., Winborn, B., Freibaum, B.D., Kanagaraj, A., et al. (2014). Axonal transport of TDP-43 mRNA granules is impaired by ALS-causing mutations. Neuron *81*, 536–543. https://doi.org/10.1016/j.neuron.2013.12.018.

Altman, T., Ionescu, A., Ibraheem, A., Priesmann, D., Gradus-Pery, T., Farberov, L., Alexandra, G., Shelestovich, N., Dafinca, R., Shomron, N., et al. (2021). Axonal TDP-43 condensates drive neuromuscular junction disruption through inhibition of local synthesis of nuclear encoded mitochondrial proteins. Nat. Commun. *12*, 6914. https://doi.org/10.1038/s41467-021-27221-8.

Amoroso, M.W., Croft, G.F., Williams, D.J., O'Keeffe, S., Carrasco, M.A., Davis, A.R., Roybon, L., Oakley, D.H., Maniatis, T., Henderson, C.E., et al. (2013). Accelerated high-yield generation of limb-innervating motor neurons from human stem cells. J. Neurosci. *33*, 574–586. https://doi.org/10.1523/JNEUROSCI.0906-12.2013.

Arai, T., Hasegawa, M., Akiyama, H., Ikeda, K., Nonaka, T., Mori, H., Mann, D., Tsuchiya, K., Yoshida, M., Hashizume, Y., et al. (2006). TDP-43 is a component of ubiquitin-positive tau-negative inclusions in frontotemporal lobar degeneration and amyotrophic lateral sclerosis. Biochem. Biophys. Res. Commun. *351*, 602–611. https://doi.org/10.1016/j.bbrc.2006.10.093.

Armstrong, G.A.B., and Drapeau, P. (2013). Calcium channel agonists protect against neuromuscular dysfunction in a genetic model of TDP-43 mutation in ALS. J. Neurosci. *33*, 1741–1752. https://doi.org/10.1523/JNEUROSCI.4003-12.2013.

Ayala, Y.M., De Conti, L., Avendaño-Vázquez, S.E., Dhir, A., Romano, M., D'Ambrogio, A., Tollervey, J., Ule, J., Baralle, M., Buratti, E., et al. (2011). TDP-43 regulates its mRNA levels through a negative feedback loop. EMBO J. *30*, 277–288. https://doi.org/10.1038/emboj.2010.310.

Baldelli, P., Fassio, A., Valtorta, F., and Benfenati, F. (2007). Lack of synapsin I reduces the readily releasable pool of synaptic vesicles at central inhibitory synapses. J. Neurosci. *27*, 13520–13531. https://doi.org/10.1523/JNEUROSCI.3151-07.2007.

Bilican, B., Serio, A., Barmada, S.J., Nishimura, A.L., Sullivan, G.J., Carrasco, M., Phatnani, H.P., Puddifoot, C.A., Story, D., Fletcher, J., et al. (2012). Mutant induced pluripotent stem cell lines recapitulate aspects of TDP-43 proteinopathies and reveal cell-specific vulnerability. Proc. Natl. Acad. Sci. U. S. A. *109*, 5803–5808. https://doi.org/10.1073/pnas.1202922109.

Blasco, H., Mavel, S., Corcia, P., and Gordon, P.H. (2014). The glutamate hypothesis in ALS: Pathophysiology and drug development. Curr. Med. Chem. *21*, 3551–3575. https://doi.org/10.2174/0929867321666140916120118.

Bossolasco, P., Sassone, F., Gumina, V., Peverelli, S., Garzo, M., and Silani, V. (2018). Motor

neuron differentiation of iPSCs obtained from peripheral blood of a mutant TARDBP ALS patient. Stem Cell Res. *30*, 61–68. https://doi.org/10.1016/j.scr.2018.05.009.

Brown, A., Wilkins, O.G., Keuss, M.J., Hill, S.E., Zanovello, M., Lee, W.C., Bampton, A., Lee, F.C.Y., Masino, L., Qi, Y.A., et al. (2022). TDP-43 loss and ALS-risk SNPs drive mis-splicing and depletion of UNC13A. Nature *603*, 131–137. https://doi.org/10.1038/s41586-022-04436-3.

Buratti, E., and Baralle, F.E. (2001). Characterization and functional implications of the RNA binding properties of nuclear factor TDP-43, a novel splicing regulator of CFTR exon 9. J. Biol. Chem. *276*, 36337–36343. https://doi.org/10.1074/jbc.M104236200.

Castellanos-Montiel, M.J., Chaineau, M., Franco-Flores, A.K., Haghi, G., Carrillo-Valenzuela, D., Reintsch, W.E., Chen, C.X.-Q., and Durcan, T.M. (2023). An optimized workflow to generate and characterize iPSC-derived motor neuron (MN) spheroids. Cells *12*, 545. https://doi.org/10.3390/cells12040545.

Chen, C.X.Q., Abdian, N., Maussion, G., Thomas, R.A., Demirova, I., Cai, E., Tabatabaei, M., Beitel, L.K., Karamchandani, J., Fon, E.A., et al. (2021). A multistep workflow to evaluate newly generated iPSCs and their ability to generate different cell types. Methods Protoc. *4*, 50. https://doi.org/10.3390/mps4030050.

Coyne, A.N., Siddegowda, B.B., Estes, P.S., Johannesmeyer, J., Kovalik, T., Daniel, S.G., Pearson, A., Bowser, R., and Zarnescu, D.C. (2014). FUTSCH/MAP1B mRNA is a translational target of TDP-43 and is neuroprotective in a Drosophila model of amyotrophic lateral sclerosis. J. Neurosci. *34*, 15962–15974. https://doi.org/10.1523/JNEUROSCI.2526-14.2014.

Coyne, A.N., Lorenzini, I., Chou, C.-C., Torvund, M., Rogers, R.S., Starr, A., Zaepfel, B.L., Levy, J., Johannesmeyer, J., Schwartz, J.C., et al. (2017). Post-transcriptional inhibition of Hsc70-4/HSPA8 expression leads to synaptic vesicle cycling defects in multiple models of ALS. Cell Rep. *21*, 110–125. https://doi.org/10.1016/j.celrep.2017.09.028.

Dafinca, R., Barbagallo, P., Farrimond, L., Candalija, A., Scaber, J., Ababneh, N.A., Sathyaprakash, C., Vowles, J., Cowley, S.A., and Talbot, K. (2020). Impairment of mitochondrial calcium buffering links mutations in C9ORF72 and TARDBP in iPS-derived motor neurons from patients with ALS/FTD. Stem Cell Reports *14*, 892–908. https://doi.org/10.1016/j.stemcr.2020.03.023.

Delestrée, N., Manuel, M., Iglesias, C., Elbasiouny, S.M., Heckman, C.J., and Zytnicki, D. (2014). Adult spinal motoneurones are not hyperexcitable in a mouse model of inherited amyotrophic lateral sclerosis. J. Physiol. *592*, 1687–1703. https://doi.org/10.1113/jphysiol.2013.265843.

Deneault, E., Chaineau, M., Nicouleau, M., Castellanos Montiel, M.J., Franco Flores, A.K., Haghi, G., Chen, C.X.Q., Abdian, N., Shlaifer, I., Beitel, L.K., et al. (2022). A streamlined CRISPR workflow to introduce mutations and generate isogenic iPSCs for modeling amyotrophic lateral sclerosis. Methods *203*, 297–310. https://doi.org/10.1016/j.ymeth.2021.09.002.

Devlin, A.-C., Burr, K., Borooah, S., Foster, J.D., Cleary, E.M., Geti, I., Vallier, L., Shaw, C.E., Chandran, S., and Miles, G.B. (2015). Human iPSC-derived motoneurons harbouring TARDBP or C9ORF72 ALS mutations are dysfunctional despite maintaining viability. Nat. Commun. *6*, 5999. https://doi.org/10.1038/ncomms6999.

Du, Z.W., Chen, H., Liu, H., Lu, J., Qian, K., Huang, C.T.L., Zhong, X., Fan, F., and Zhang, S.C. (2015). Generation and expansion of highly pure motor neuron progenitors from human pluripotent stem cells. Nat. Commun. *6*, 6626. https://doi.org/10.1038/ncomms7626.

Egawa, N., Kitaoka, S., Tsukita, K., Naitoh, M., Takahashi, K., Yamamoto, T., Adachi, F., Kondo, T., Okita, K., Asaka, I., et al. (2012). Drug screening for ALS using patient-specific induced pluripotent stem cells. Sci. Transl. Med. *4*, 145ra104. https://doi.org/10.1126/scitranslmed.3004052.

Estes, P.S., Boehringer, A., Zwick, R., Tang, J.E., Grigsby, B., and Zarnescu, D.C. (2011). Wild-type and A315T mutant TDP-43 exert differential neurotoxicity in a Drosophila model of ALS. Hum. Mol. Genet. *20*, 2308–2321. https://doi.org/10.1093/hmg/ddr124.

Fazal, R., Boeynaems, S., Swijsen, A., De Decker, M., Fumagalli, L., Moisse, M., Vanneste, J., Guo, W., Boon, R., Vercruysse, T., et al. (2021). HDAC6 inhibition restores TDP-43 pathology and axonal transport defects in human motor neurons with TARDBP mutations. EMBO J. *40*, 1–24. https://doi.org/10.15252/embj.2020106177.

Fuchs, A., Kutterer, S., Mühling, T., Duda, J., Schütz, B., Liss, B., Keller, B.U., and Roeper, J. (2013). Selective mitochondrial Ca 2+ uptake deficit in disease endstage vulnerable motoneurons of the SOD1 G93A mouse model of amyotrophic lateral sclerosis. J. Physiol. *591*, 2723–2745. https://doi.org/10.1113/jphysiol.2012.247981.

Fujimori, K., Ishikawa, M., Otomo, A., Atsuta, N., Nakamura, R., Akiyama, T., Hadano, S., Aoki, M., Saya, H., Sobue, G., et al. (2018). Modeling sporadic ALS in iPSC-derived motor neurons identifies a potential therapeutic agent. Nat. Med. *24*, 1579–1589. https://doi.org/10.1038/s41591-018-0140-5.

Gulino, R. (2023). Synaptic dysfunction and plasticity in amyotrophic lateral sclerosis. Int. J. Mol. Sci. *24*, 4613. https://doi.org/10.3390/ijms24054613.

Guo, W., Naujock, M., Fumagalli, L., Vandoorne, T., Baatsen, P., Boon, R., Ordovás, L., Patel, A., Welters, M., Vanwelden, T., et al. (2017). HDAC6 inhibition reverses axonal transport defects in motor neurons derived from FUS-ALS patients. Nat. Commun. *8*, 861. https://doi.org/10.1038/s41467-017-00911-y.

Hawrot, J., Imhof, S., and Wainger, B.J. (2020). Modeling cell-autonomous motor neuron phenotypes in ALS using iPSCs. Neurobiol. Dis. *134*, 104680. https://doi.org/10.1016/j.nbd.2019.104680.

Iguchi, Y., Katsuno, M., Niwa, J., Takagi, S., Ishigaki, S., Ikenaka, K., Kawai, K., Watanabe, H., Yamanaka, K., Takahashi, R., et al. (2013). Loss of TDP-43 causes age-dependent progressive motor neuron degeneration. Brain *136*, 1371–1382. https://doi.org/10.1093/brain/awt029.

Imaizumi, K., Ideno, H., Sato, T., Morimoto, S., and Okano, H. (2022). Pathogenic mutation of TDP-43 impairs RNA processing in a cell type-specific manner: Implications for the pathogenesis of ALS/FTLD. ENeuro *9*, 1–12. https://doi.org/10.1523/ENEURO.0061-22.2022.

Kabashi, E., Lin, L., Tradewell, M.L., Dion, P.A., Bercier, V., Bourgouin, P., Rochefort, D., Bel Hadj, S., Durham, H.D., Velde, C. Vande, et al. (2010). Gain and loss of function of ALS-related mutations of TARDBP (TDP-43) cause motor deficits in vivo. Hum. Mol. Genet. *19*, 671–683. https://doi.org/10.1093/hmg/ddp534.

Kenna, K.P., McLaughlin, R.L., Byrne, S., Elamin, M., Heverin, M., Kenny, E.M., Cormican, P., Morris, D.W., Donaghy, C.G., Bradley, D.G., et al. (2013). Delineating the genetic heterogeneity of ALS using targeted high-throughput sequencing. J. Med. Genet. *50*, 776–783. https://doi.org/10.1136/jmedgenet-2013-101795.

Kilpinen, H., Goncalves, A., Leha, A., Afzal, V., Alasoo, K., Ashford, S., Bala, S., Bensaddek, D.,

Casale, F.P., Culley, O.J., et al. (2017). Common genetic variation drives molecular heterogeneity in human iPSCs. Nature *546*, 370–375. https://doi.org/10.1038/nature22403.

Kim, B.W., Ryu, J., Jeong, Y.E., Kim, J., and Martin, L.J. (2020). Human motor neurons with SOD1-G93A mutation generated from CRISPR/Cas9 gene-edited iPSCs develop pathological features of amyotrophic lateral sclerosis. Front. Cell. Neurosci. *14*, 1–16. https://doi.org/10.3389/fncel.2020.604171.

Klim, J.R., Williams, L.A., Limone, F., Guerra San Juan, I., Davis-Dusenbery, B.N., Mordes, D.A., Burberry, A., Steinbaugh, M.J., Gamage, K.K., Kirchner, R., et al. (2019). ALS-implicated protein TDP-43 sustains levels of STMN2, a mediator of motor neuron growth and repair. Nat. Neurosci. *22*, 167–179. https://doi.org/10.1038/s41593-018-0300-4.

Krach, F., Wheeler, E.C., Regensburger, M., Boerstler, T., Wend, H., Vu, A.Q., Wang, R., Reischl, S., Boldt, K., Batra, R., et al. (2022). Aberrant NOVA1 function disrupts alternative splicing in early stages of amyotrophic lateral sclerosis. Acta Neuropathol. *144*, 413–435. https://doi.org/10.1007/s00401-022-02450-3.

Kraemer, B.C., Schuck, T., Wheeler, J.M., Robinson, L.C., Trojanowski, J.Q., Lee, V.M.Y., and Schellenberg, G.D. (2010). Loss of murine TDP-43 disrupts motor function and plays an essential role in embryogenesis. Acta Neuropathol. *119*, 409–419. https://doi.org/10.1007/s00401-010-0659-0.

Kreiter, N., Pal, A., Lojewski, X., Corcia, P., Naujock, M., Reinhardt, P., Sterneckert, J., Petri, S., Wegner, F., Storch, A., et al. (2018). Age-dependent neurodegeneration and organelle transport deficiencies in mutant TDP43 patient-derived neurons are independent of TDP43 aggregation. Neurobiol. Dis. *115*, 167–181. https://doi.org/10.1016/j.nbd.2018.03.010.

Lépine, S., Castellanos-Montiel, M.J., and Durcan, T.M. (2022). TDP-43 dysregulation and neuromuscular junction disruption in amyotrophic lateral sclerosis. Transl. Neurodegener. *11*, 1–24. https://doi.org/10.1186/s40035-022-00331-z.

Ling, S.-C. (2018). Synaptic paths to neurodegeneration: The emerging role of TDP-43 and FUS in synaptic functions. Neural Plast. *2018*, 1–13. https://doi.org/10.1155/2018/8413496.

Ma, X.R., Prudencio, M., Koike, Y., Vatsavayai, S.C., Kim, G., Harbinski, F., Briner, A., Rodriguez, C.M., Guo, C., Akiyama, T., et al. (2022). TDP-43 represses cryptic exon inclusion in the FTD–ALS gene UNC13A. Nature *603*, 124–130. https://doi.org/10.1038/s41586-022-04424-7.

Mackenzie, I.R.A., Bigio, E.H., Ince, P.G., Geser, F., Neumann, M., Cairns, N.J., Kwong, L.K., Forman, M.S., Ravits, J., Stewart, H., et al. (2007). Pathological TDP-43 distinguishes sporadic amyotrophic lateral sclerosis from amyotrophic lateral sclerosis with SOD1 mutations. Ann. Neurol. *61*, 427–434. https://doi.org/10.1002/ana.21147.

de Majo, M., Koontz, M., Marsan, E., Salinas, N., Ramsey, A., Kuo, Y.-M., Seo, K., Li, H., Dräger, N., Leng, K., et al. (2023). Granulin loss of function in human mature brain organoids implicates astrocytes in TDP-43 pathology. Stem Cell Reports *13*, 1–15. https://doi.org/10.1016/j.stemcr.2023.01.012.

Martínez-Silva, M. de L., Imhoff-Manuel, R.D., Sharma, A., Heckman, C., Shneider, N.A., Roselli, F., Zytnicki, D., and Manuel, M. (2018). Hypoexcitability precedes denervation in the large fast-contracting motor units in two unrelated mouse models of ALS. Elife *7*, e30955. https://doi.org/10.7554/eLife.30955.

Masrori, P., and Van Damme, P. (2020). Amyotrophic lateral sclerosis: a clinical review. Eur. J. Neurol. *27*, 1918–1929. https://doi.org/10.1111/ene.14393.

Mishra, M., Paunesku, T., Woloschak, G.E., Siddique, T., Zhu, L., Lin, S., Greco, K., and Bigio, E.H. (2007). Gene expression analysis of frontotemporal lobar degeneration of the motor neuron disease type with ubiquitinated inclusions. Acta Neuropathol. *114*, 81–94. https://doi.org/10.1007/s00401-007-0240-7.

Mitchell, J.C., Constable, R., So, E., Vance, C., Scotter, E., Glover, L., Hortobagyi, T., Arnold, E.S., Ling, S.-C., McAlonis, M., et al. (2015). Wild type human TDP-43 potentiates ALS-linked mutant TDP-43 driven progressive motor and cortical neuron degeneration with pathological features of ALS. Acta Neuropathol. Commun. *3*, 36. https://doi.org/10.1186/s40478-015-0212-4.

Mollinari, C., Zhao, J., Lupacchini, L., Garaci, E., Merlo, D., and Pei, G. (2018). Transdifferentiation: a new promise for neurodegenerative diseases. Cell Death Dis. *9*, 830. https://doi.org/10.1038/s41419-018-0891-4.

Moura, M.C., Novaes, M.R.C.G., Eduardo, E.J., Zago, Y.S.S.P., Freitas, R.D.N.B., and Casulari, L.A. (2015). Prognostic factors in amyotrophic lateral sclerosis: A population-based study. PLoS One *10*, e0141500. https://doi.org/10.1371/journal.pone.0141500.

Naujock, M., Stanslowsky, N., Bufler, S., Naumann, M., Reinhardt, P., Sterneckert, J., Kefalakes, E., Kassebaum, C., Bursch, F., Lojewski, X., et al. (2016). 4-Aminopyridine induced activity rescues hypoexcitable motor neurons from amyotrophic lateral sclerosis patient-derived induced pluripotent stem cells. Stem Cells *34*, 1563–1575. https://doi.org/10.1002/stem.2354.

Neumann, M., Sampathu, D.M., Kwong, L.K., Truax, A.C., Micsenyi, M.C., Chou, T.T., Bruce, J., Schuck, T., Grossman, M., Clark, C.M., et al. (2006). Ubiquitinated TDP-43 in frontotemporal lobar degeneration and amyotrophic lateral sclerosis. Science (80-.). *314*, 130–133. https://doi.org/10.1126/science.1134108.

Ou, S.H., Wu, F., Harrich, D., García-Martínez, L.F., and Gaynor, R.B. (1995). Cloning and characterization of a novel cellular protein, TDP-43, that binds to human immunodeficiency virus type 1 TAR DNA sequence motifs. J. Virol. *69*, 3584–3596. https://doi.org/10.1128/jvi.69.6.3584-3596.1995.

Pereira, J.D., DuBreuil, D.M., Devlin, A.-C., Held, A., Sapir, Y., Berezovski, E., Hawrot, J., Dorfman, K., Chander, V., and Wainger, B.J. (2021). Human sensorimotor organoids derived from healthy and amyotrophic lateral sclerosis stem cells form neuromuscular junctions. Nat. Commun. *12*, 4744. https://doi.org/10.1038/s41467-021-24776-4.

Polymenidou, M., Lagier-Tourenne, C., Hutt, K.R., Huelga, S.C., Moran, J., Liang, T.Y., Ling, S.-C., Sun, E., Wancewicz, E., Mazur, C., et al. (2011). Long pre-mRNA depletion and RNA missplicing contribute to neuronal vulnerability from loss of TDP-43. Nat. Neurosci. *14*, 459–468. https://doi.org/10.1038/nn.2779.

Ratti, A., Gumina, V., Lenzi, P., Bossolasco, P., Fulceri, F., Volpe, C., Bardelli, D., Pregnolato, F., Maraschi, A., Fornai, F., et al. (2020). Chronic stress induces formation of stress granules and pathological TDP-43 aggregates in human ALS fibroblasts and iPSC-motoneurons. Neurobiol. Dis. *145*, 105051. https://doi.org/10.1016/j.nbd.2020.105051.

Rosahl, T.W., Spillane, D., Missler, M., Herz, J., Selig, D.K., Wolff, J.R., Hammer, R.E., Malenka, R.C., and Südhof, T.C. (1995). Essential functions of synapsins I and II in synaptic vesicle regulation. Nature *375*, 488–493. https://doi.org/10.1038/375488a0.

Rothstein, J.D., Martin, L.J., and Kuncl, R.W. (1992). Decreased glutamate transport by the brain and spinal cord in amyotrophic lateral sclerosis. N. Engl. J. Med. *326*, 1464–1468. https://doi.org/10.1056/NEJM199205283262204.

Rothstein, J.D., Van Kammen, M., Levey, A.I., Martin, L.J., and Kuncl, R.W. (1995). Selective loss of glial glutamate transporter GLT-1 in amyotrophic lateral sclerosis. Ann. Neurol. *38*, 73–84. https://doi.org/10.1002/ana.410380114.

Rouhani, F., Kumasaka, N., de Brito, M.C., Bradley, A., Vallier, L., and Gaffney, D. (2014). Genetic background drives transcriptional variation in human induced pluripotent stem cells. PLoS Genet. *10*, e1004432. https://doi.org/10.1371/journal.pgen.1004432.

Sareen, D., O'Rourke, J.G., Meera, P., Muhammad, A.K.M.G., Grant, S., Simpkinson, M., Bell, S., Carmona, S., Ornelas, L., Sahabian, A., et al. (2013). Targeting RNA foci in iPSC-derived motor neurons from ALS patients with a C9ORF72 repeat expansion. Sci. Transl. Med. *5*, 208ra149. https://doi.org/10.1126/scitranslmed.3007529.

Seminary, E.R., Sison, S.L., and Ebert, A.D. (2018). Modeling protein aggregation and the heat shock response in ALS iPSC-derived motor neurons. Front. Neurosci. *12*, 1–15. https://doi.org/10.3389/fnins.2018.00086.

Sephton, C.F., Good, S.K., Atkin, S., Dewey, C.M., Mayer, P., Herz, J., and Yu, G. (2010). TDP-43 is a developmentally regulated protein essential for early embryonic development. J. Biol. Chem. *285*, 6826–6834. https://doi.org/10.1074/jbc.M109.061846.

Shan, X., Chiang, P.-M., Price, D.L., and Wong, P.C. (2010). Altered distributions of Gemini of coiled bodies and mitochondria in motor neurons of TDP-43 transgenic mice. Proc. Natl. Acad. Sci. *107*, 16325–16330. https://doi.org/10.1073/pnas.1003459107.

Shi, Y., Hung, S.T., Rocha, G., Lin, S., Linares, G.R., Staats, K.A., Seah, C., Wang, Y., Chickering, M., Lai, J., et al. (2019). Identification and therapeutic rescue of autophagosome and glutamate receptor defects in C9ORF72 and sporadic ALS neurons. JCI Insight *4*, 1–21. https://doi.org/10.1172/jci.insight.127736.

Smith, A.S.T., Chun, C., Hesson, J., Mathieu, J., Valdmanis, P.N., Mack, D.L., Choi, B.O., Kim, D.H., and Bothwell, M. (2021). Human induced pluripotent stem cell-derived TDP-43 mutant neurons exhibit consistent functional phenotypes across multiple gene edited lines despite transcriptomic and splicing discrepancies. Front. Cell Dev. Biol. *9*, 1–18. https://doi.org/10.3389/fcell.2021.728707.

Sun, X., Song, J., Huang, H., Chen, H., and Qian, K. (2018). Modeling hallmark pathology using motor neurons derived from the family and sporadic amyotrophic lateral sclerosis patient-specific iPS cells. Stem Cell Res. Ther. *9*, 315. https://doi.org/10.1186/s13287-018-1048-1.

Vucic, S., Nicholson, G.A., and Kiernan, M.C. (2008). Cortical hyperexcitability may precede the onset of familial amyotrophic lateral sclerosis. Brain *131*, 1540–1550. https://doi.org/10.1093/brain/awn071.

Wainger, B.J., Kiskinis, E., Mellin, C., Wiskow, O., Han, S.S.W., Sandoe, J., Perez, N.P., Williams, L.A., Lee, S., Boulting, G., et al. (2014). Intrinsic membrane hyperexcitability of amyotrophic lateral sclerosis patient-derived motor neurons. Cell Rep. *7*, 1–11. https://doi.org/10.1016/j.celrep.2014.03.019.

Wang, W., Li, L., Lin, W.-L., Dickson, D.W., Petrucelli, L., Zhang, T., and Wang, X. (2013). The ALS disease-associated mutant TDP-43 impairs mitochondrial dynamics and function in motor

neurons. Hum. Mol. Genet. *22*, 4706–4719. https://doi.org/10.1093/hmg/ddt319.

Weskamp, K., Tank, E.M., Miguez, R., McBride, J.P., Gómez, N.B., White, M., Lin, Z., Gonzalez, C.M., Serio, A., Sreedharan, J., et al. (2020). Shortened TDP43 isoforms upregulated by neuronal hyperactivity drive TDP43 pathology in ALS. J. Clin. Invest. *130*, 1139–1155. https://doi.org/10.1172/JCI130988.

Wu, L.-S., Cheng, W.-C., and Shen, C.-K.J. (2012). Targeted depletion of TDP-43 expression in the spinal cord motor neurons leads to the development of amyotrophic lateral sclerosis-like phenotypes in mice. J. Biol. Chem. *287*, 27335–27344. https://doi.org/10.1074/jbc.M112.359000.

Yang, C., Wang, H., Qiao, T., Yang, B., Aliaga, L., Qiu, L., Tan, W., Salameh, J., McKenna-Yasek, D.M., Smith, T., et al. (2014). Partial loss of TDP-43 function causes phenotypes of amyotrophic lateral sclerosis. Proc. Natl. Acad. Sci. *111*, E1121–E1129. https://doi.org/10.1073/pnas.1322641111.

Zhang, Z., Almeida, S., Lu, Y., Nishimura, A.L., Peng, L., Sun, D., Wu, B., Karydas, A.M., Tartaglia, M.C., Fong, J.C., et al. (2013). Downregulation of microRNA-9 in iPSC-derived neurons of FTD/ALS patients with TDP-43 mutations. PLoS One *8*, e76055. https://doi.org/10.1371/journal.pone.0076055.

Zhao, C., Devlin, A., Chouhan, A.K., Selvaraj, B.T., Stavrou, M., Burr, K., Brivio, V., He, X., Mehta, A.R., Story, D., et al. (2020). Mutant C9orf72 human iPSC-derived astrocytes cause non-cell autonomous motor neuron pathophysiology. Glia *68*, 1046–1064. https://doi.org/10.1002/glia.23761.

Zuo, X., Zhou, J., Li, Y., Wu, K., Chen, Z., Luo, Z., Zhang, X., Liang, Y., Esteban, M.A., Zhou, Y., et al. (2021). TDP-43 aggregation induced by oxidative stress causes global mitochondrial imbalance in ALS. Nat. Struct. Mol. Biol. *28*, 132–142. https://doi.org/10.1038/s41594-020-00537-7.

Figures

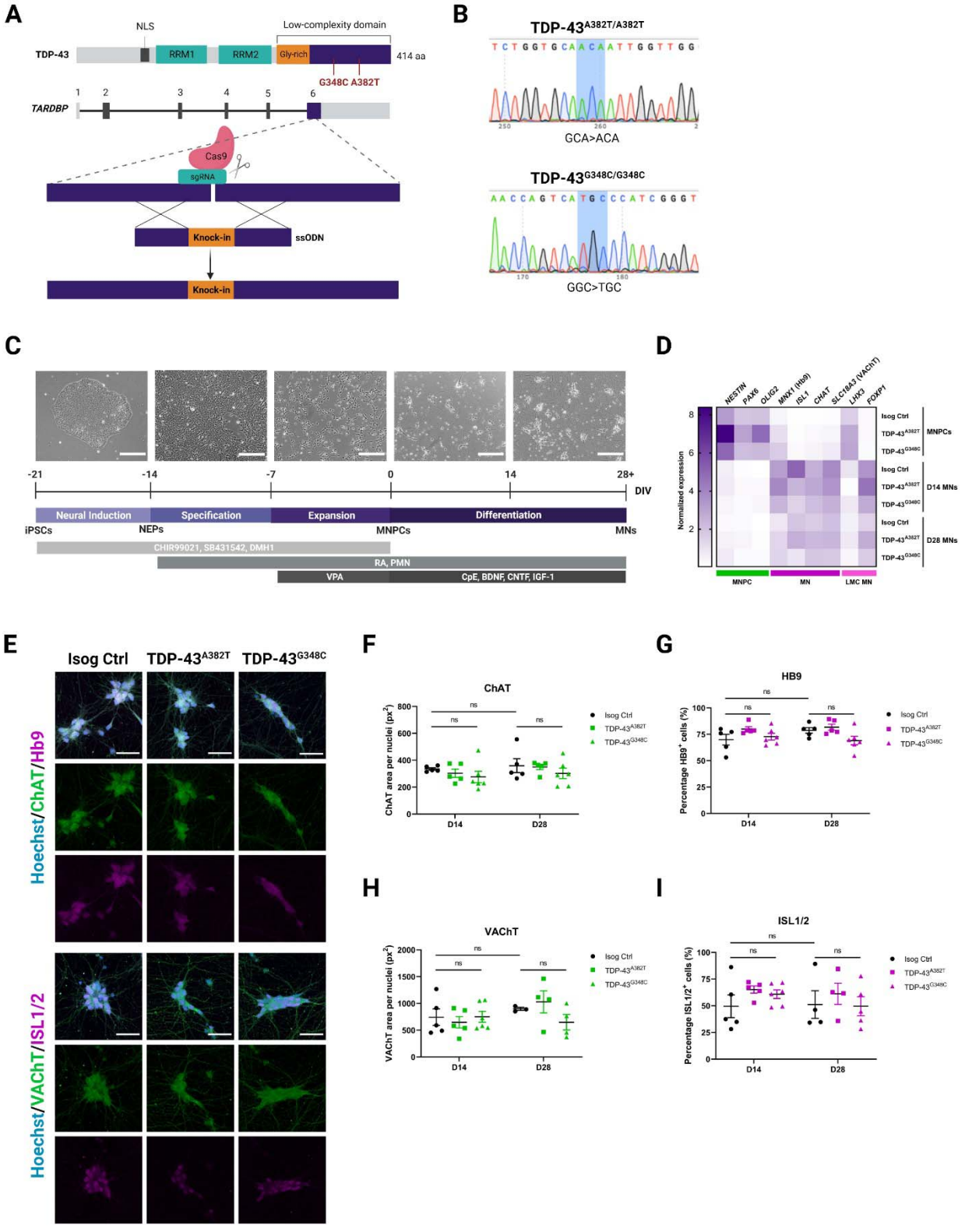

Figure 1. Generation of *TARDBP* knock-in iPSC lines and differentiation into MNs.

(A) Schematic representation of CRISPR/Cas9-mediated genome editing via homology-directed repair.

(B) iPSC lines genotyping using Sanger sequencing.

(C) Schematic representation of the protocol for sequential differentiation of iPSCs into neuroepithelial progenitors (NEPs), MNPCs, and MNs with representative phase-contrast images of cells along differentiation. Scale bar, 250 µm. For time-lapse movie depicting maturation of MNPCs into MNs, see Video 1.

(D) qPCR heatmap showing normalized transcripts levels of MNPC (green), MN (purple), and LMC (pink) markers during differentiation of MNPCs into MNs. Mean plotted. n=3 independent experiments.

(E-I) Representative images (E) and quantification (F-I) of MNs differentiated for 2 weeks (D14) and 4 weeks (D28) subjected to immunocytochemistry for the common MN markers Hb9, ISL1/2, ChAT and VAChT. Scale bar, 50 µm. Data shown as mean ± SEM. n=5 independent experiments.

See also Figures S1 to S3.

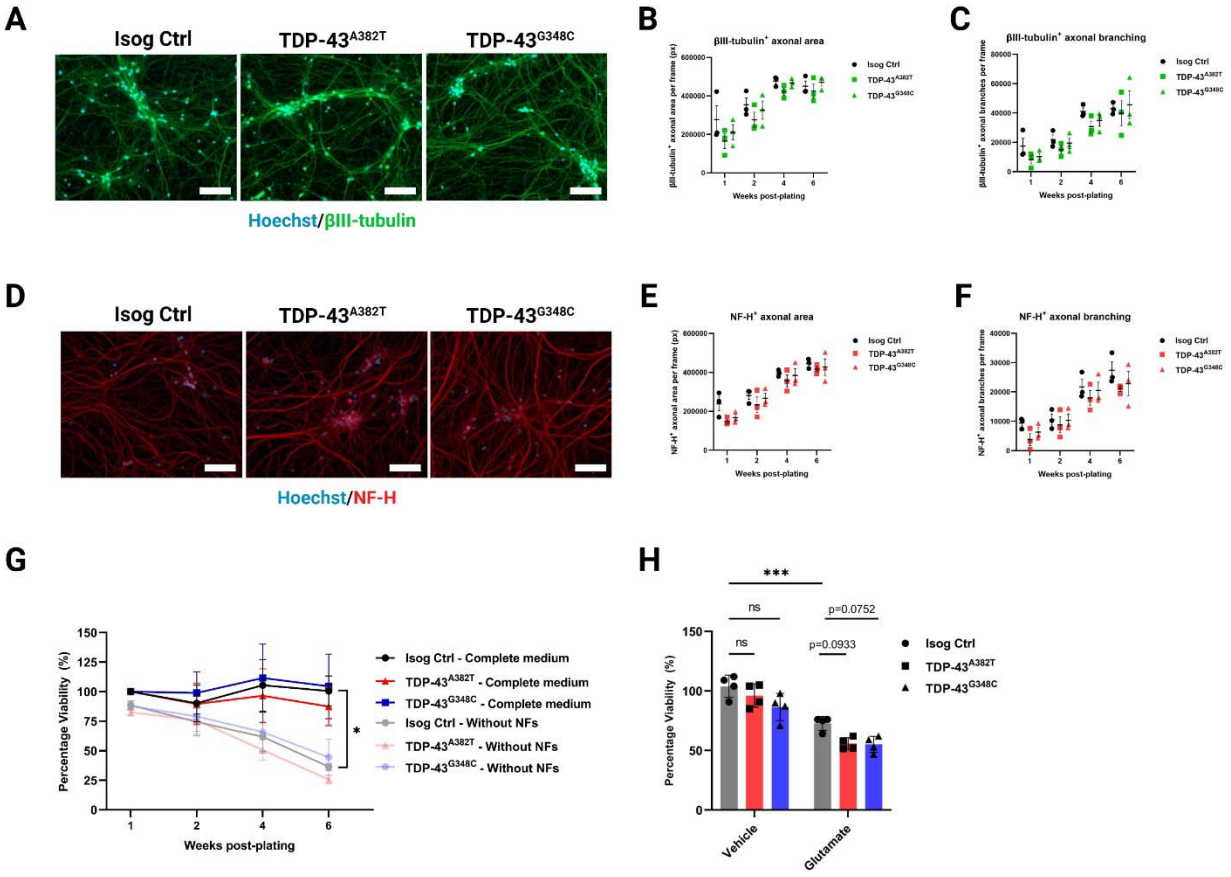

Figure 2. TDP-43 MN cultures form a normal axonal network and maintain viability.

(A,D) Representative images of MNs differentiated for 6 weeks subjected to immunocytochemistry for neuronal markers βIII-tubulin (A) and NF-H (D). Scale bar, 100 µm.

(B,C) Quantification of total area (B) and number of branches (C) of βIII-tubulin^{+} axons. n=3 independent experiments.

(E,F) Quantification of total area (E) and number of branches (F) of NF-H^{+} axons. n=3 independent experiments.

(G) Viability of MN cultures differentiated with and without neurotrophic factor (NF) supplementation over a span of 6 weeks post-plating. n=4 independent experiments.

(H) Effect of glutamate treatment (0.1 mM glutamate, 24 h) on viability of MNs differentiated for 6 weeks. n=4 independent experiments.

All data shown as mean ± SEM. *p<0.05, **p<0.01, ***p<0.001.

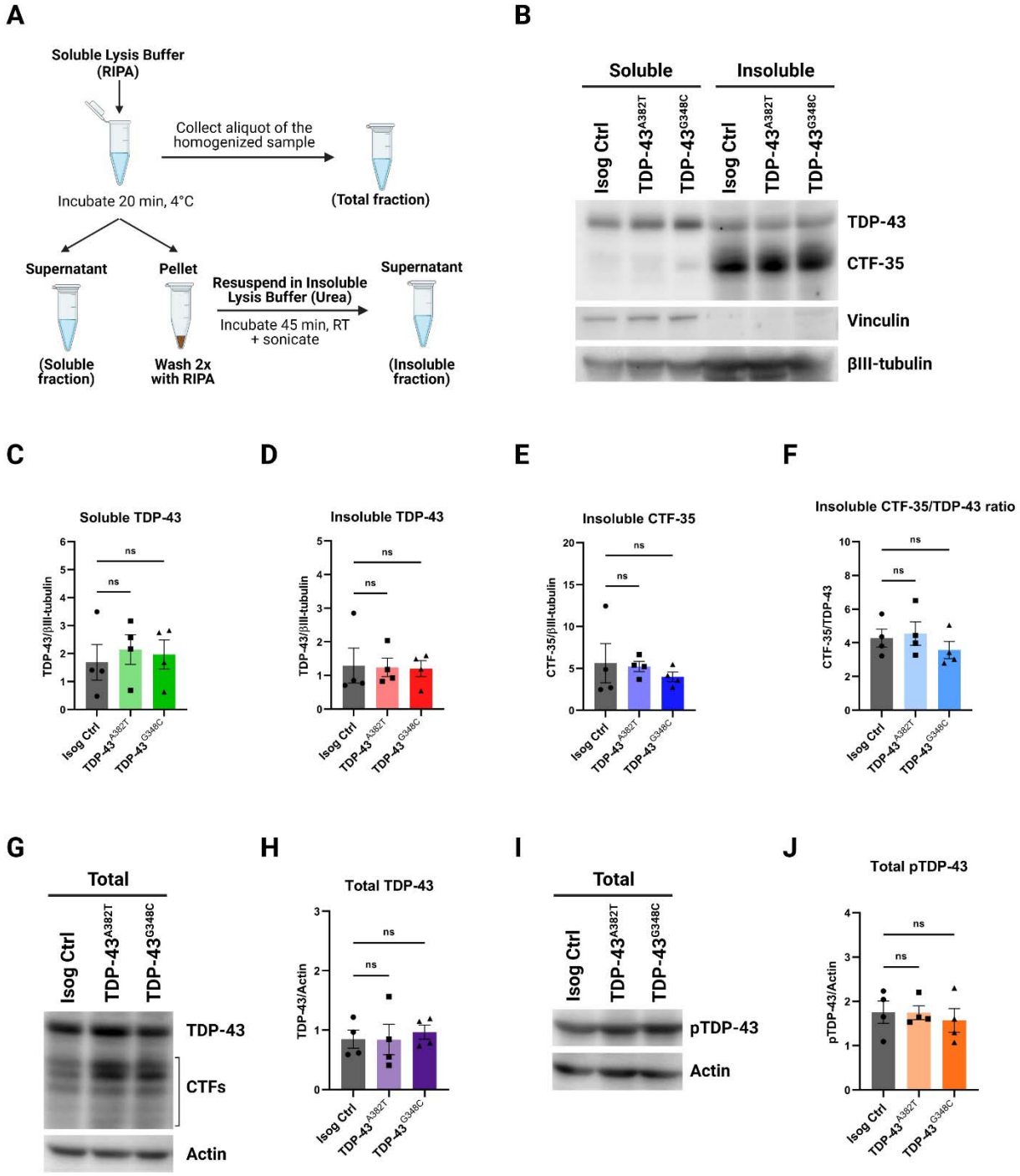

Figure 3. Quantification of TDP-43 levels in total, soluble, and insoluble protein fractions.

(A) Schematics representing the fractionation workflow into total (unfractionated), soluble (RIPA), and insoluble (urea) protein fractions.

(B-F) Immunoblot (B) and quantification of TDP-43 (C, D) and C-terminal fragment of 35 kDa (CTF-35) (E, F) levels in soluble and insoluble fractions. Vinculin (soluble) and βIII-tubulin were used as fractionation and loading controls, respectively.

(G-J) Immunoblot (G, I) and quantification of total levels of TDP-43 (H) and phosphorylated TDP-43 (Ser409/410) (J) in unfractionated lysates. Actin was used as loading control.

All data shown as mean ± SEM. Extractions were performed in in MNs harvested at 6 weeks post-plating. n=4 independent experiments. See also Figure S4.

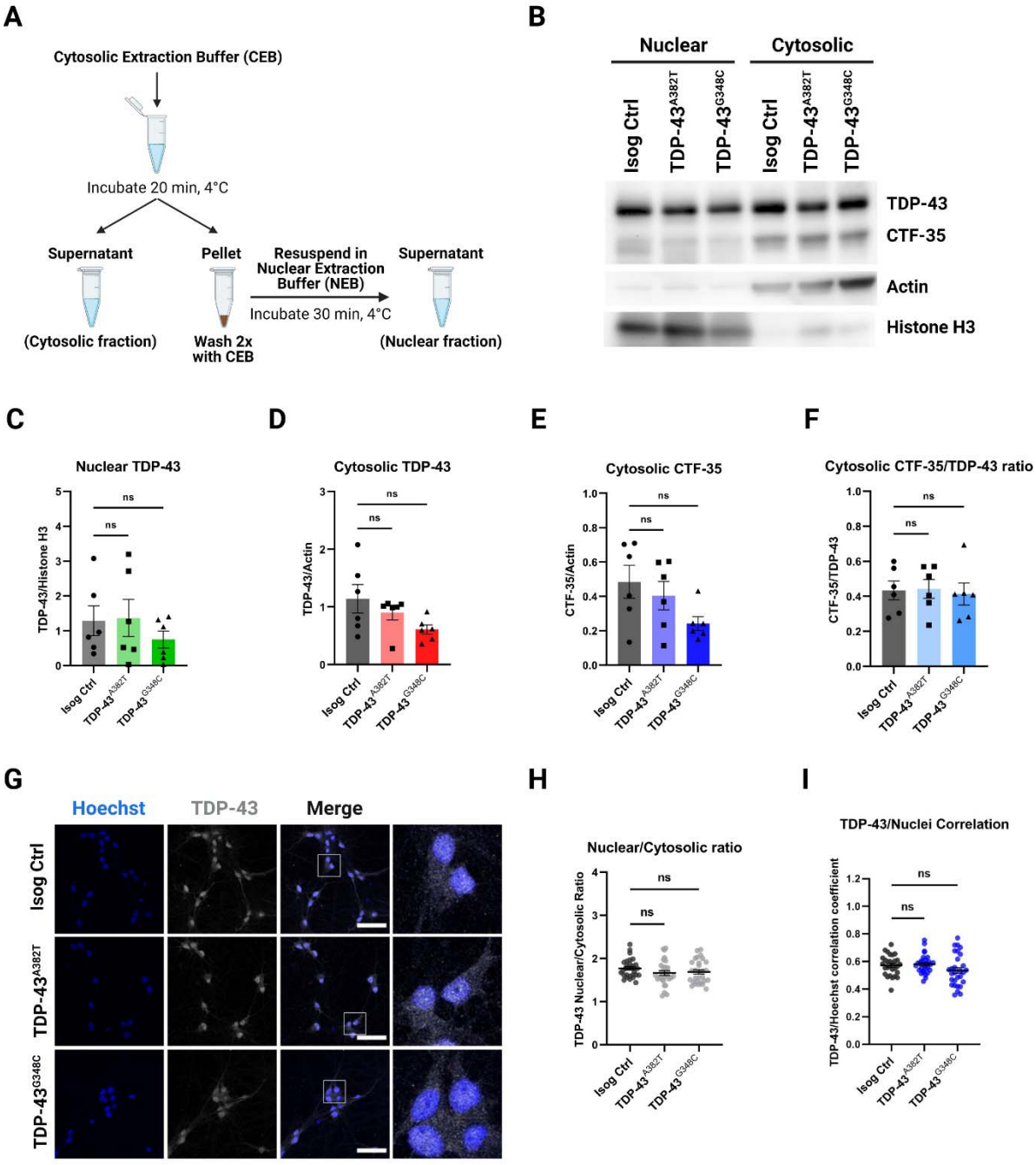

Figure 4. Subcellular distribution of TDP-43 in MNs.

(A) Schematics representing the fractionation workflow into nuclear and cytosolic fractions.

(B-F) Immunoblot of nuclear and cytosolic fractions (B) and quantification of nuclear (C) and cytosolic (D) TDP-43 levels, and cytosolic C-terminal fragment of 35 kDa (CTF-35) levels (E and

F). Histone H3 (nuclear marker) and actin (cytosolic marker) were used as both loading and fractionation controls. n=6 extractions from 4 independent differentiations. Pooled data from MNs harvested 4- and 6-weeks post-plating.

(G) Representative images of MNs differentiated for 6 weeks subjected to immunocytochemistry for TDP-43 (C-terminal antibody). Scale bar, 50 µm.

(H, I) Quantification of TDP-43 distribution using the nuclear/cytosolic ratio of TDP-43 fluorescence signal intensity (H) and the TDP-43/Hoechst correlation coefficient (I). Individual data points represent per-frame mean values from 5 independent experiments.

All data shown as mean ± SEM. See also Figure S5.

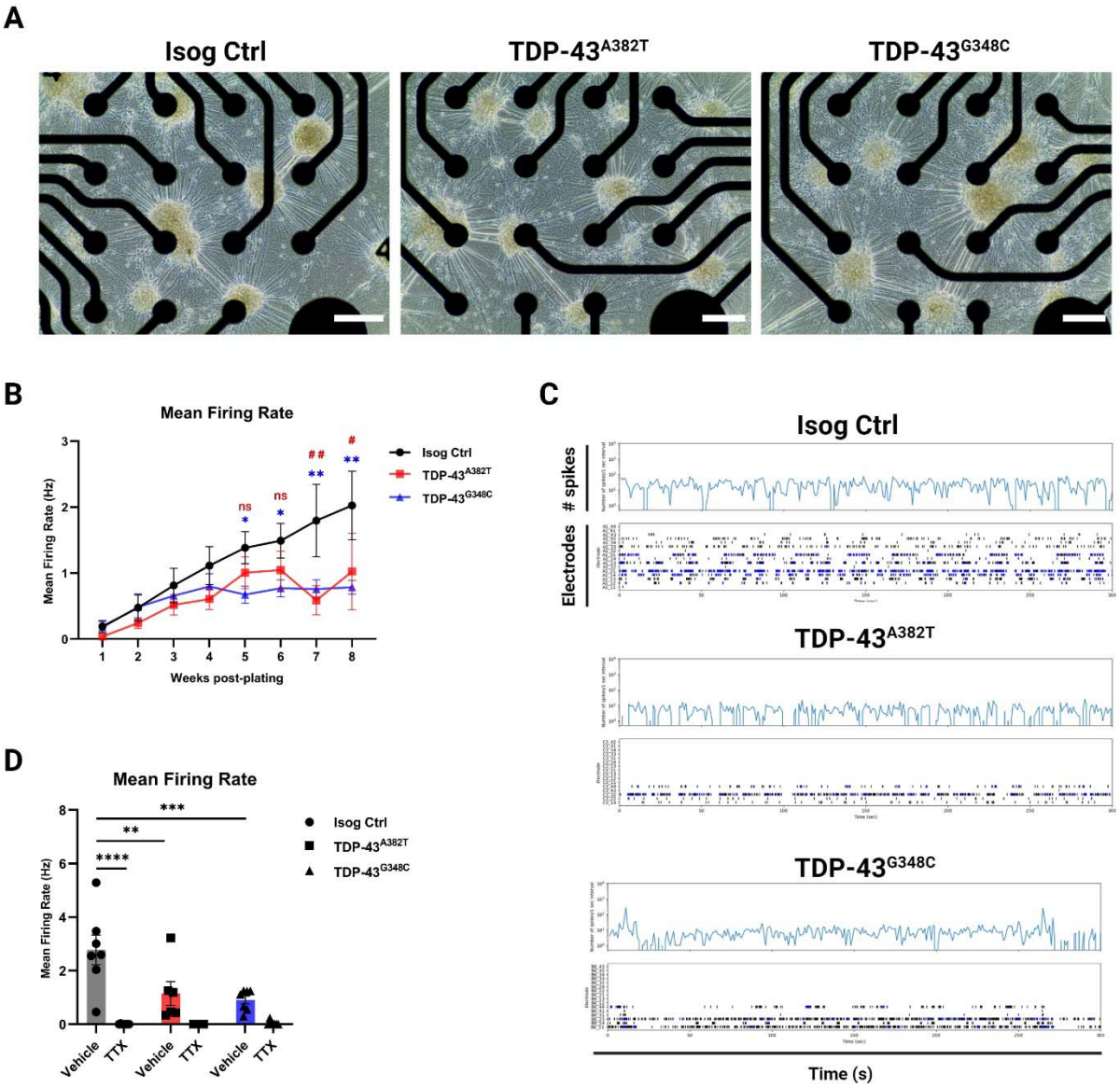

Figure 5. TDP-43 MNs show progressive alterations in spontaneous neuronal activity.

(A) Representative phase-contrast images of MNs differentiated for 6 weeks on 24-well MEA plates. Scale bar, 250 µm**.**

(B) Longitudinal changes in mean firing rate of MNs recorded weekly over a span of 8 weeks post-plating. n=11 independent experiments.

(C) Spontaneous neuronal activity of MN cultures differentiated for 6 weeks recorded for 300s shown as raster plot and spike histogram. Individual spikes are shown in black and bursts are shown in blue.

(D) Effect of TTX treatment on mean firing rate in MNs differentiated for 6 weeks. n=7 independent experiments.

All data shown as mean ± SEM. *p<0.05, **p<0.01, ***p<0.001, ****p<0.0001. See also Figure S6.

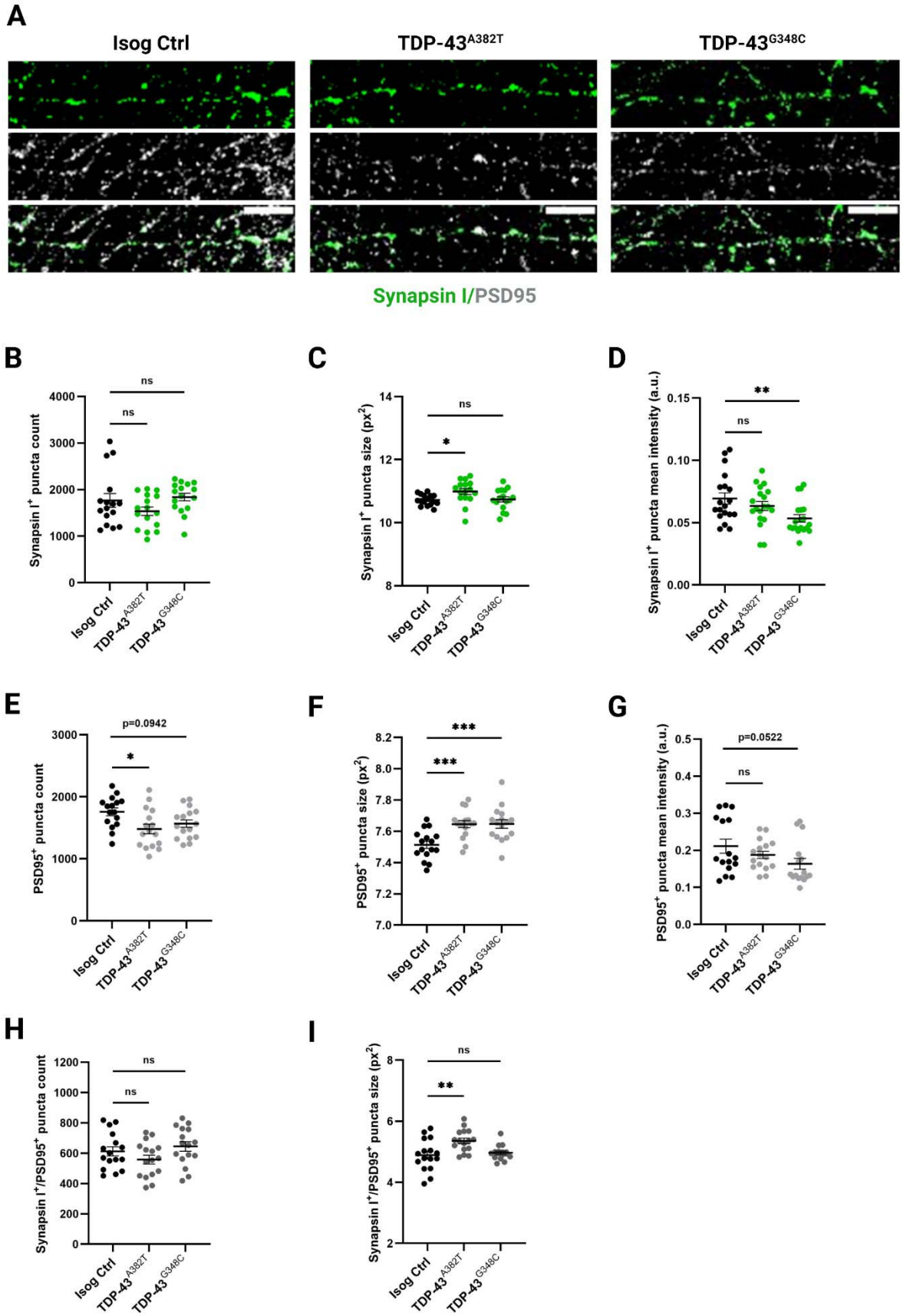

Figure 6. TDP-43 MNs exhibit synaptic abnormalities.

(A) Representative images of 6 weeks post-plating MN neurites subjected to immunocytochemistry for synapsin I and PSD95. Scale bar, 10 µm.

(B-D) Quantification of the average number (B), size (C), and intensity (D) of synapsin I^+ puncta.

(E-G) Quantification of the average number (E), size (F), and intensity (G) of $PSD95^+$ puncta.

(H,I) Quantification of the average number (H), and size (I) of synapsin I^+/$PSD95^+$ puncta.

Individual points represent per-frame values from 3 independent experiments.

All data shown as mean ± SEM. *p<0.05, **p<0.01, ***p<0.001.

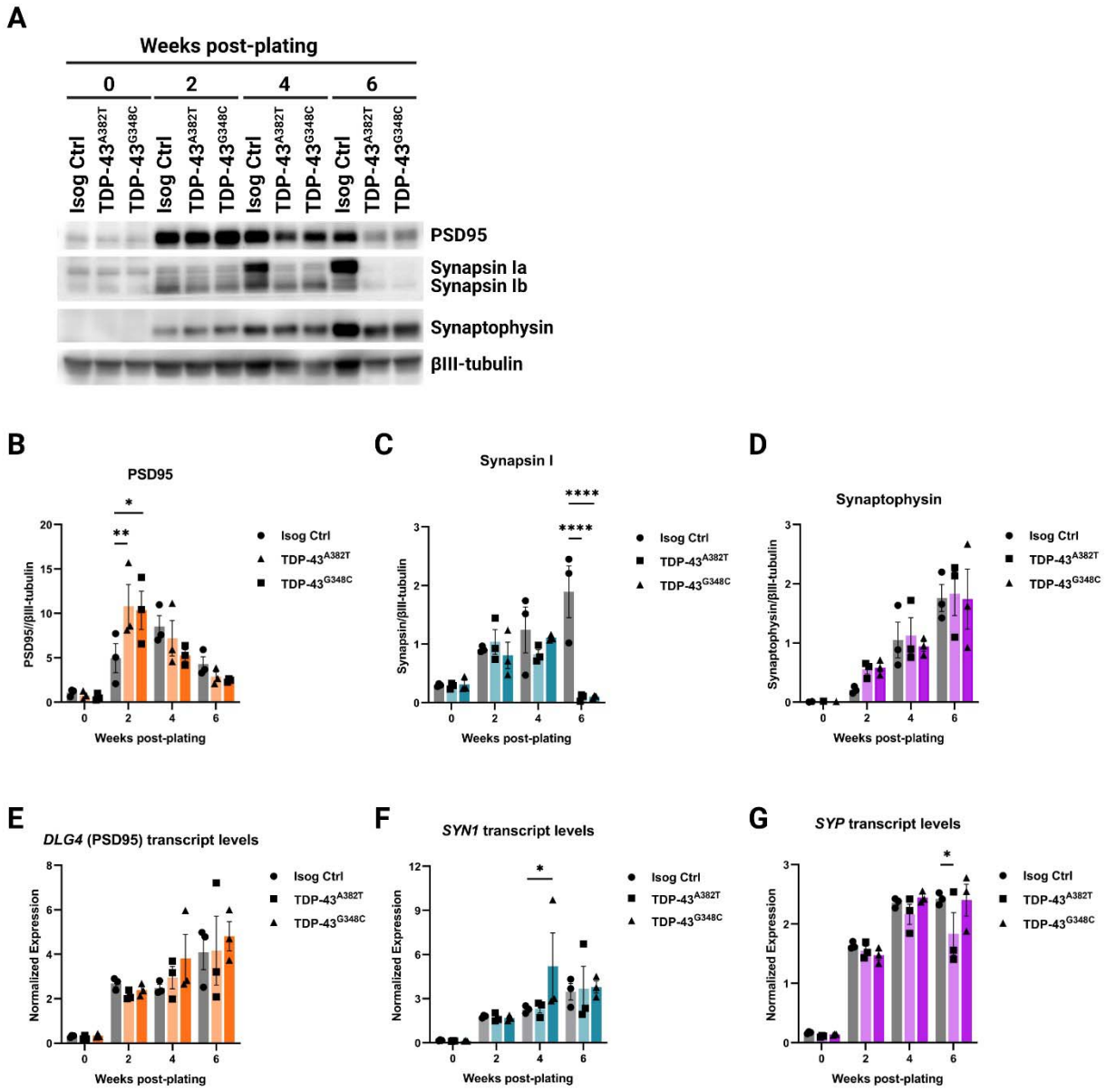

Figure 7. TDP-43 variants lead to decreased synapsin I protein levels but not *SYN1* transcript levels.

(A-D) Immunoblot (A) and quantification of protein levels of PSD95 (B), synapsin I (C), and synaptophysin (D) in MNPCs and MNs harvested after 2, 4, and 6 weeks of differentiation. βIII-tubulin was used as loading control.

(E-G) Longitudinal quantification of relative transcript levels of *DLG4* (encoding PSD95) (E), *SYN1* (F), and *SYP* (G) using qPCR.

All data shown as mean ± SEM. *p<0.05, **p<0.01, ***p<0.001, ****p<0.0001. n=3 independent experiments.

Videos

Video 1. Differentiation of MNPCs into MNs. Related to Figure 1. Time-lapse movie depicting the differentiation of MNPCs into MNs during 2 weeks post-plating. Scale bar, 150 µm.

Video 2. Electrophysiological recording of MN cultures using MEA. Related to Figure 5. Movie depicting spontaneous neuronal activity in MNs differentiated for 7 weeks using the AxIS Navigator 1.5.1.12 software (Axion Biosystems). Warmer colors indicate greater changes in local field potentials.

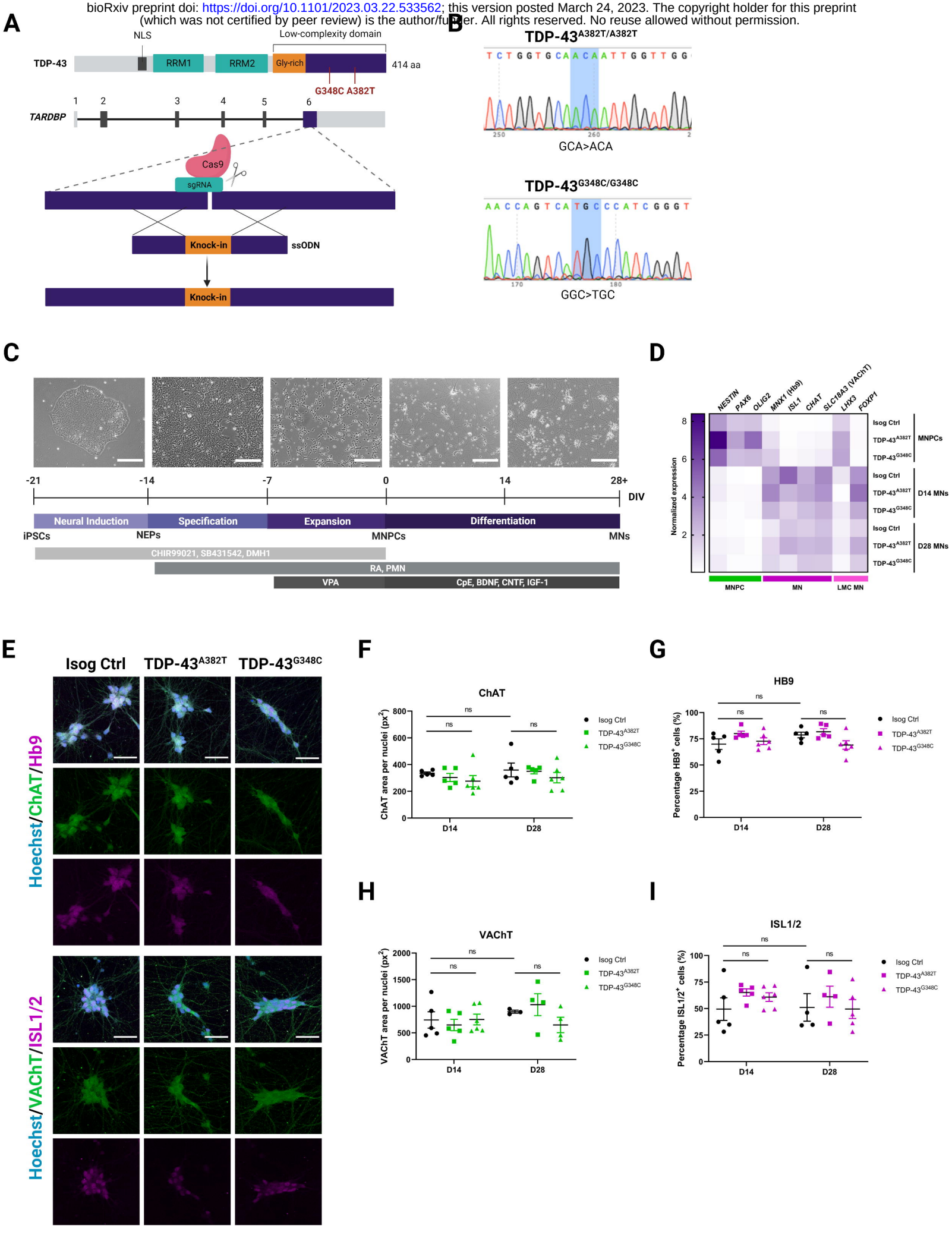

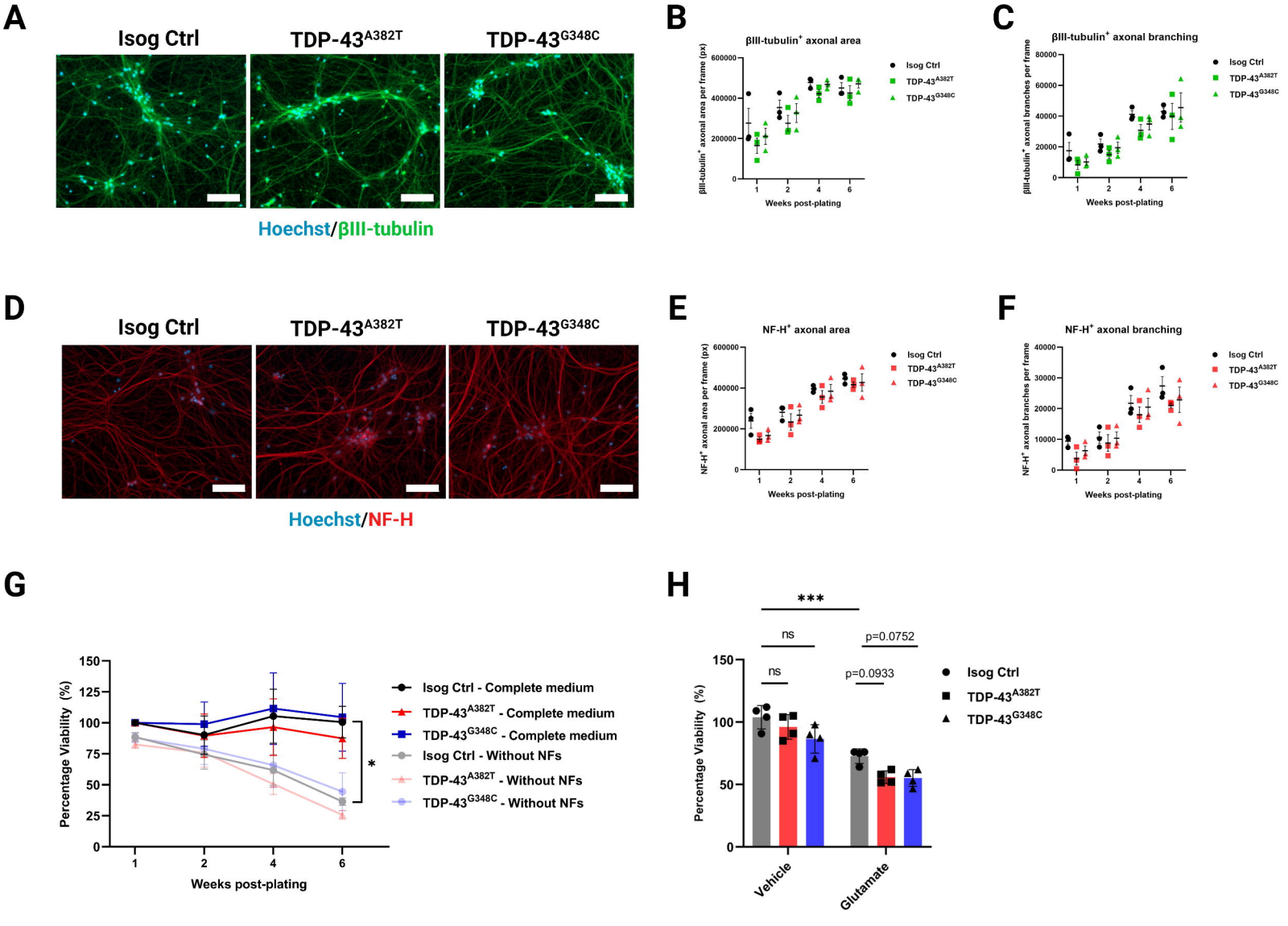
A
Isog Ctrl
TDP-43A382T
TDP-43G348C
Hoechst/βIII-tubulin
B
βIII-tubulin+ axonal area
βIII-tubulin+ axonal area per frame (px)
Weeks post-plating
Isog Ctrl
TDP-43A382T
TDP-43G348C
C
βIII-tubulin+ axonal branching
βIII-tubulin+ axonal branches per frame
Weeks post-plating
D
Isog Ctrl
TDP-43A382T
TDP-43G348C
Hoechst/NF-H
E
NF-H+ axonal area
NF-H+ axonal area per frame (px)
Weeks post-plating
F
NF-H+ axonal branching
NF-H+ axonal branches per frame
Weeks post-plating
G
Percentage Viability (%)
Weeks post-plating
Isog Ctrl - Complete medium
TDP-43A382T - Complete medium
TDP-43G348C - Complete medium
Isog Ctrl - Without NFs
TDP-43A382T - Without NFs
TDP-43G348C - Without NFs
*
H
***
ns
p=0.0752
ns
p=0.0933
Percentage Viability (%)
Vehicle
Glutamate
Isog Ctrl
TDP-43A382T
TDP-43G348C

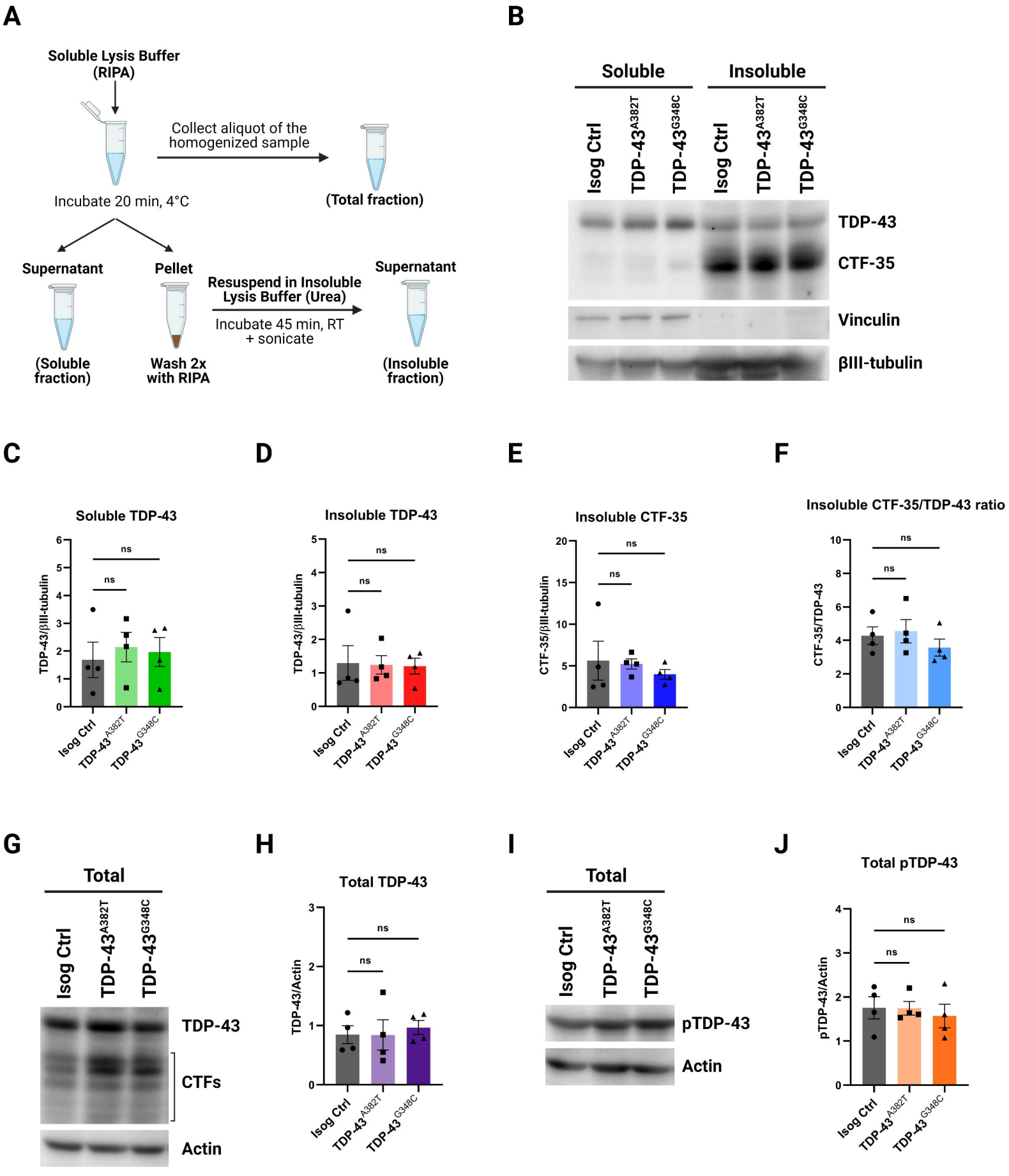
A
Soluble Lysis Buffer (RIPA)
Collect aliquot of the homogenized sample
Incubate 20 min, 4°C
(Total fraction)
Supernatant
Pellet
Resuspend in Insoluble Lysis Buffer (Urea)
Incubate 45 min, RT + sonicate
Supernatant
(Soluble fraction)
Wash 2x with RIPA
(Insoluble fraction)
B
Soluble
Insoluble
Isog Ctrl
TDP-43A382T
TDP-43G348C
Isog Ctrl
TDP-43A382T
TDP-43G348C
TDP-43
CTF-35
Vinculin
βIII-tubulin
C
Soluble TDP-43
TDP-43/βIII-tubulin
ns
ns
Isog Ctrl
TDP-43A382T
TDP-43G348C
D
Insoluble TDP-43
TDP-43/βIII-tubulin
ns
ns
Isog Ctrl
TDP-43A382T
TDP-43G348C
E
Insoluble CTF-35
CTF-35/βIII-tubulin
ns
ns
Isog Ctrl
TDP-43A382T
TDP-43G348C
F
Insoluble CTF-35/TDP-43 ratio
CTF-35/TDP-43
ns
ns
Isog Ctrl
TDP-43A382T
TDP-43G348C
G
Total
Isog Ctrl
TDP-43A382T
TDP-43G348C
TDP-43
CTFs
Actin
H
Total TDP-43
TDP-43/Actin
ns
ns
Isog Ctrl
TDP-43A382T
TDP-43G348C
I
Total
Isog Ctrl
TDP-43A382T
TDP-43G348C
pTDP-43
Actin
J
Total pTDP-43
pTDP-43/Actin
ns
ns
Isog Ctrl
TDP-43A382T
TDP-43G348C

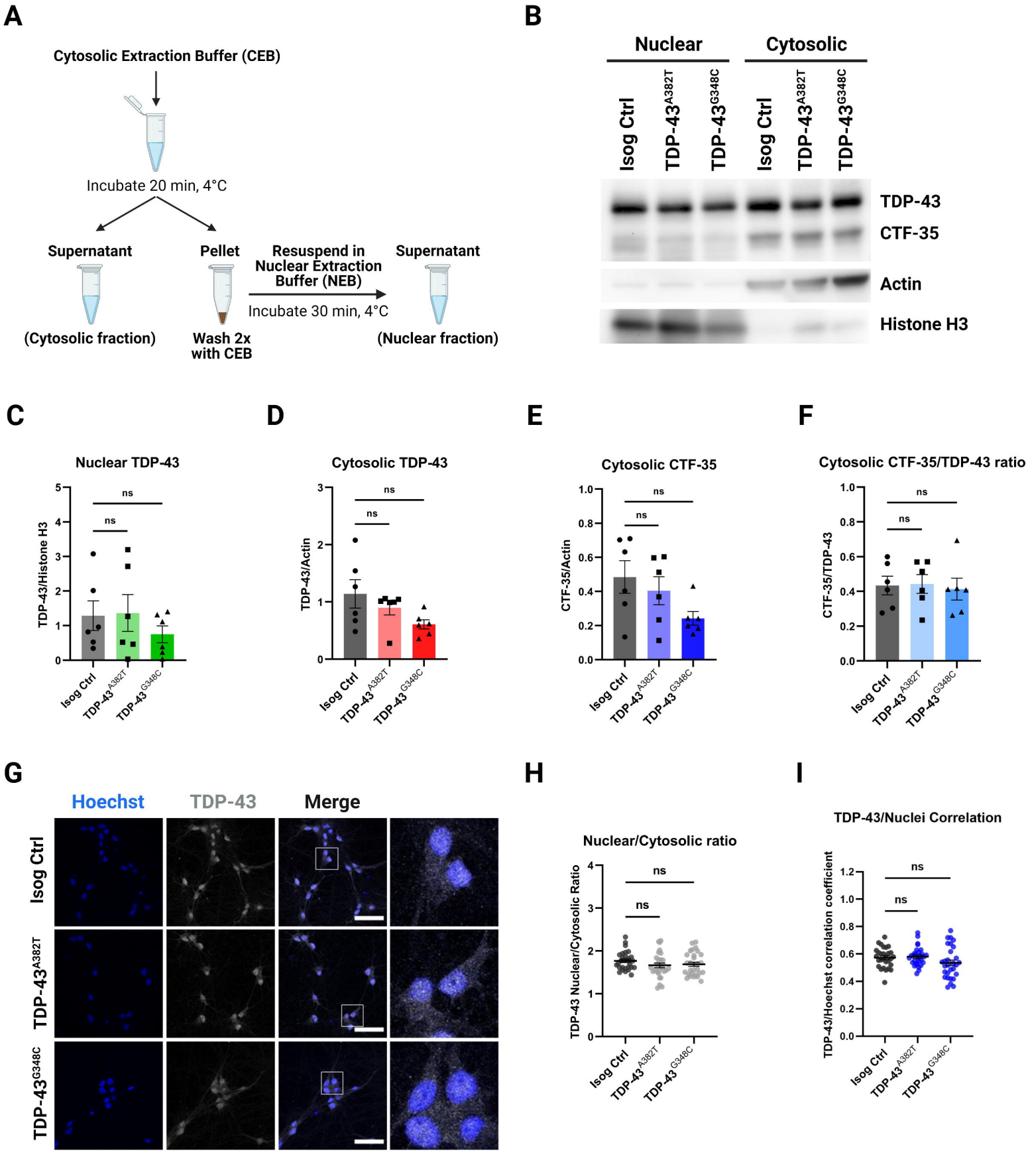
A
Cytosolic Extraction Buffer (CEB)
Incubate 20 min, 4°C
Supernatant
Pellet
Resuspend in Nuclear Extraction Buffer (NEB)
Supernatant
Incubate 30 min, 4°C
(Cytosolic fraction)
Wash 2x with CEB
(Nuclear fraction)
B
Nuclear
Cytosolic
Isog Ctrl
TDP-43A382T
TDP-43G348C
Isog Ctrl
TDP-43A382T
TDP-43G348C
TDP-43
CTF-35
Actin
Histone H3
C
Nuclear TDP-43
TDP-43/Histone H3
ns
ns
Isog Ctrl
TDP-43A382T
TDP-43G348C
D
Cytosolic TDP-43
TDP-43/Actin
ns
ns
Isog Ctrl
TDP-43A382T
TDP-43G348C
E
Cytosolic CTF-35
CTF-35/Actin
ns
ns
Isog Ctrl
TDP-43A382T
TDP-43G348C
F
Cytosolic CTF-35/TDP-43 ratio
CTF-35/TDP-43
ns
ns
Isog Ctrl
TDP-43A382T
TDP-43G348C
G
Hoechst
TDP-43
Merge
Isog Ctrl
TDP-43A382T
TDP-43G348C
H
Nuclear/Cytosolic ratio
TDP-43 Nuclear/Cytosolic Ratio
ns
ns
Isog Ctrl
TDP-43A382T
TDP-43G348C
I
TDP-43/Nuclei Correlation
TDP-43/Hoechst correlation coefficient
ns
ns
Isog Ctrl
TDP-43A382T
TDP-43G348C

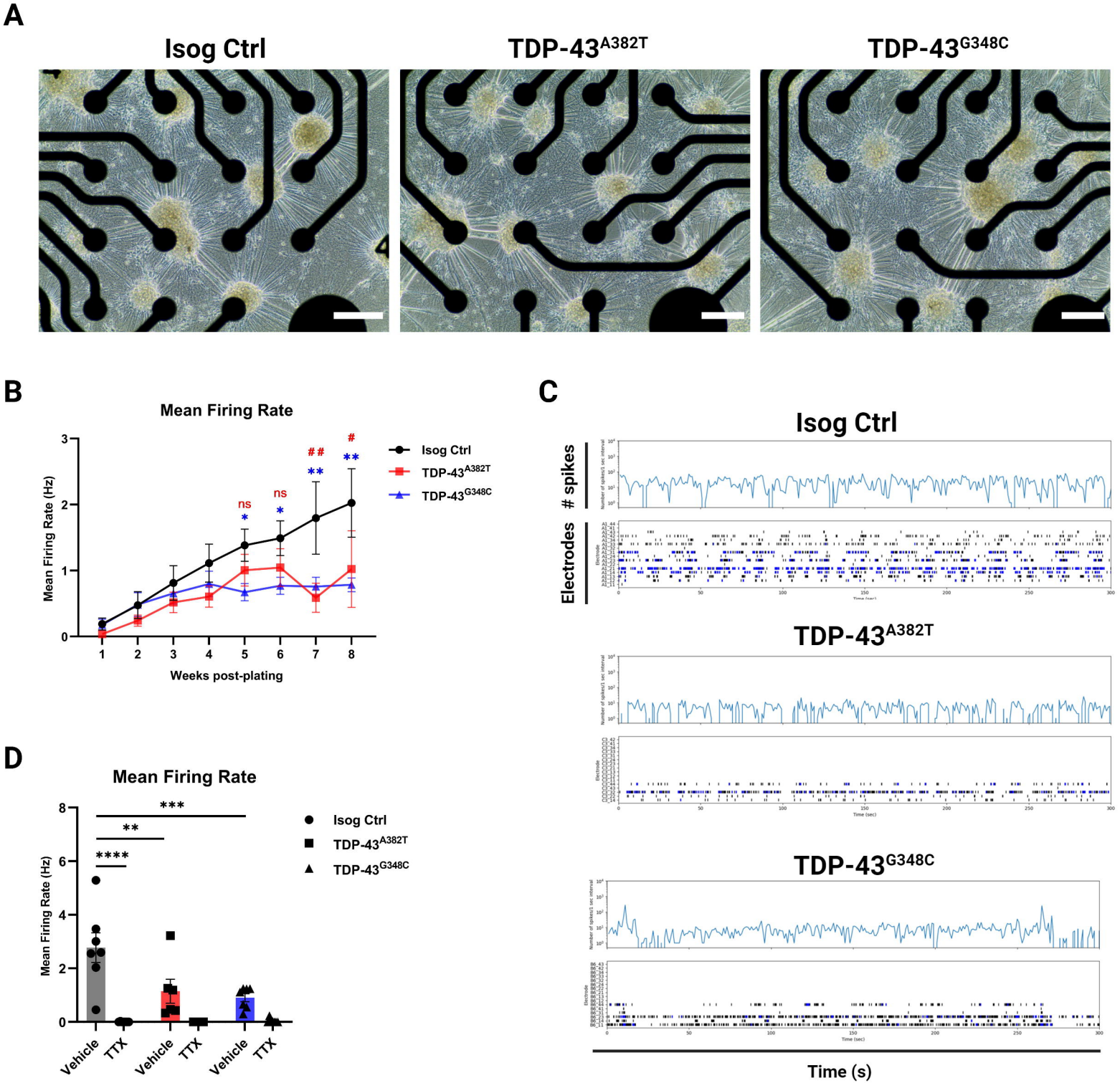
A
Isog Ctrl
TDP-43A382T
TDP-43G348C
B
Mean Firing Rate
Mean Firing Rate (Hz)
Weeks post-plating
Isog Ctrl
TDP-43A382T
TDP-43G348C
ns
ns
*
*
**
**
##
#
C
Isog Ctrl
spikes
Electrodes
TDP-43A382T
TDP-43G348C
Time (s)
D
Mean Firing Rate
Mean Firing Rate (Hz)
***
**
****
Vehicle
TTX
Vehicle
TTX
Vehicle
TTX
Isog Ctrl
TDP-43A382T
TDP-43G348C

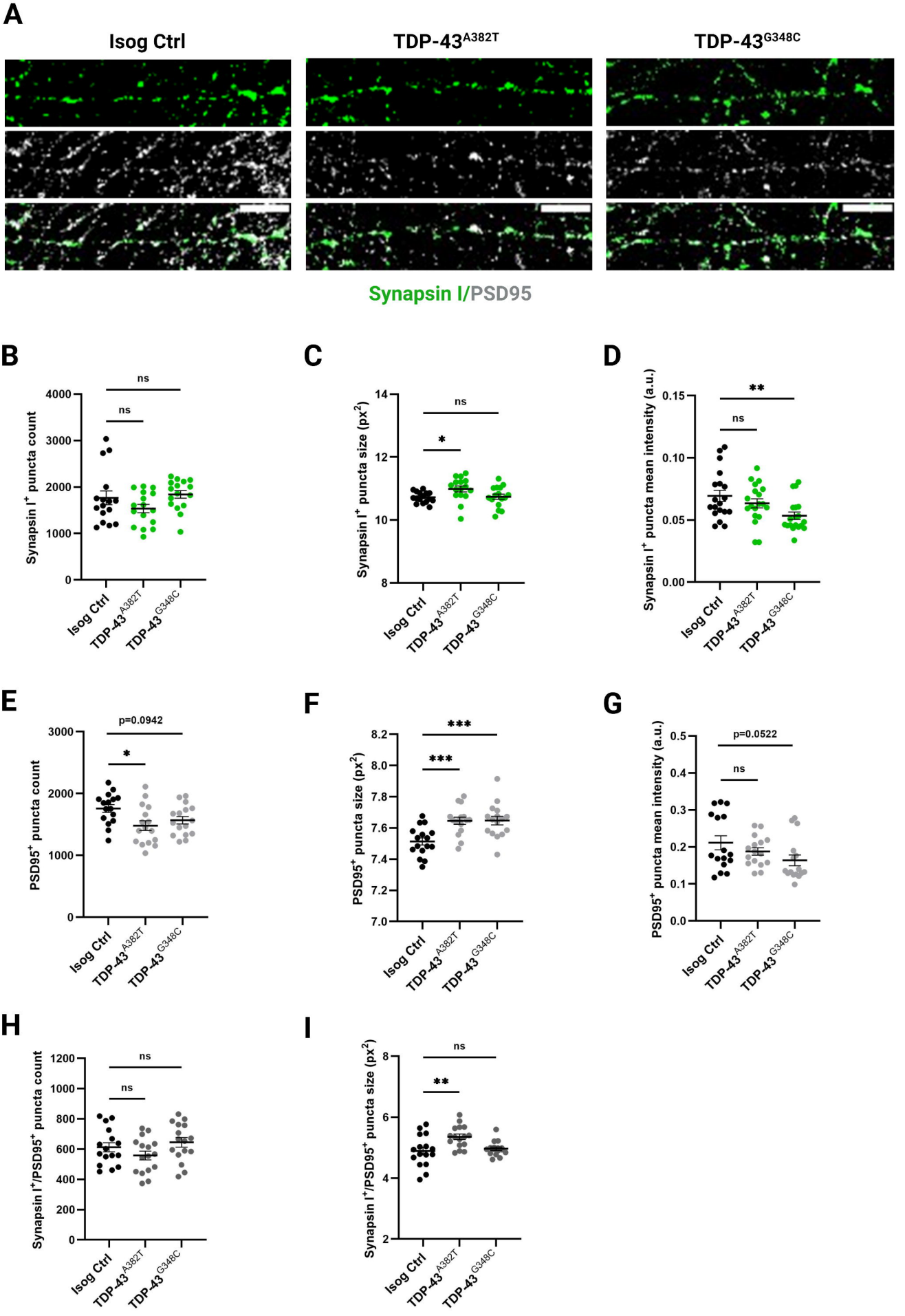
A
Isog Ctrl
TDP-43A382T
TDP-43G348C
Synapsin I/PSD95
B
Synapsin I+ puncta count
ns
ns
C
Synapsin I+ puncta size (px2)
ns
*
D
Synapsin I+ puncta mean intensity (a.u.)
**
ns
E
PSD95+ puncta count
p=0.0942
*
F
PSD95+ puncta size (px2)
***
***
G
PSD95+ puncta mean intensity (a.u.)
p=0.0522
ns
H
Synapsin I+/PSD95+ puncta count
ns
ns
I
Synapsin I+/PSD95+ puncta size (px2)
ns
**
Isog Ctrl
TDP-43A382T
TDP-43G348C

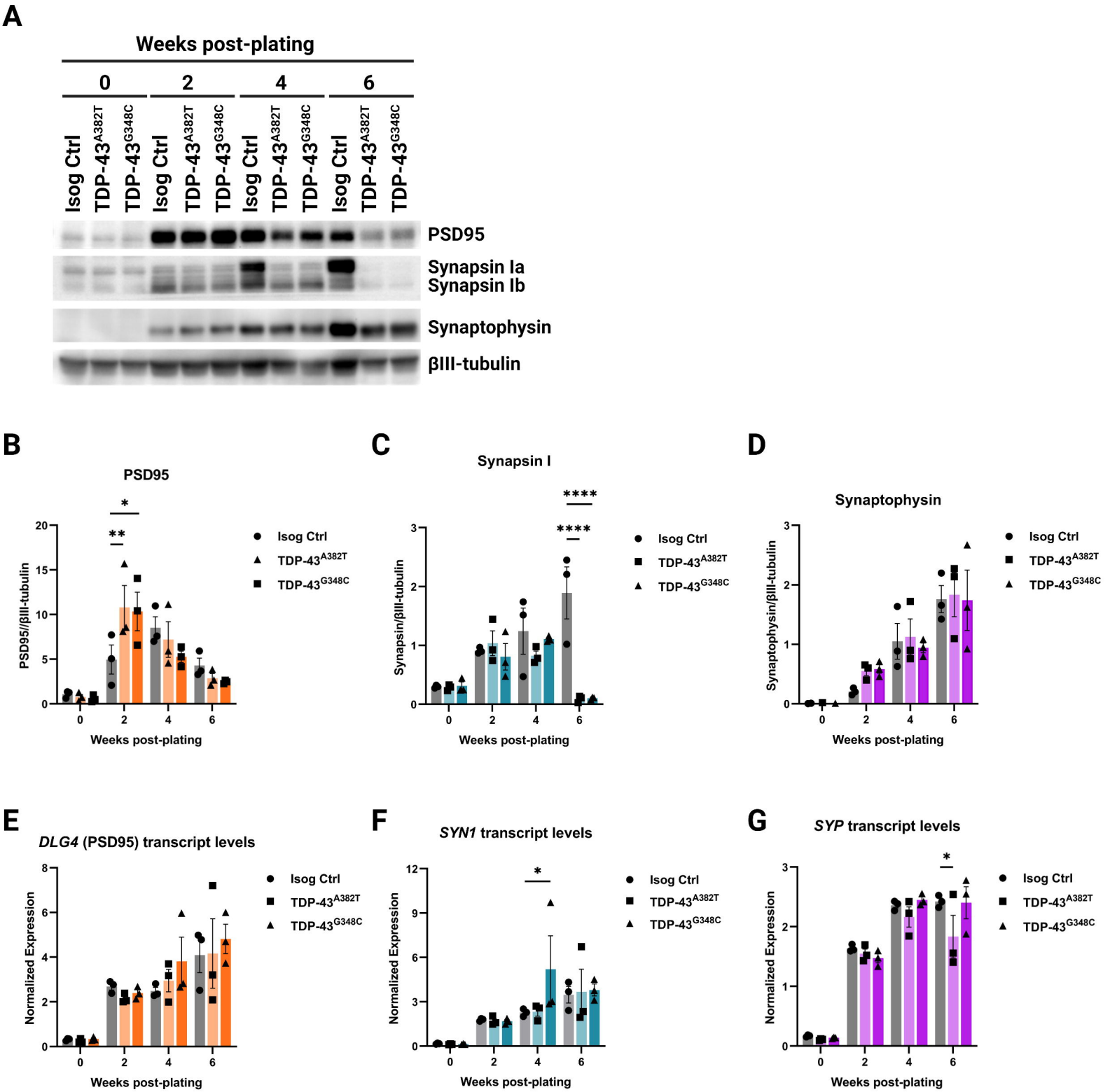
A
Weeks post-plating
0
2
4
6
Isog Ctrl
TDP-43A382T
TDP-43G348C
PSD95
Synapsin Ia
Synapsin Ib
Synaptophysin
βIII-tubulin
B
PSD95
PSD95/βIII-tubulin
Weeks post-plating
C
Synapsin I
Synapsin/βIII-tubulin
D
Synaptophysin
Synaptophysin/βIII-tubulin
E
DLG4 (PSD95) transcript levels
Normalized Expression
F
SYN1 transcript levels
G
SYP transcript levels